

Search is All You Need for Few-shot Anomaly Detection

Qishan Wang*

Academy for Engineering and
Technology
Fudan University
Shanghai, China
qswang20@fudan.edu.cn

Jia Guo*†

School of Biomedical Engineering
Tsinghua University
Beijing, China
j-g24@mails.tsinghua.edu.cn

Shuyong Gao

School of Computer Science
Fudan university
Shanghai, China
sygao18@fudan.edu.cn

Haofen Wang

College of Design & Innovation
Tongji University
Shanghai, China
carter.whfcarter@gmail.com

Li Xiong

School of Physics and Mechanical &
Electrical Engineering
Hexi University
Gansu, China
xl2025@hxu.edu.cn

Junjie Hu

School of Computer Science
Fudan university
Shanghai, China
23210240182@m.fudan.edu.cn

Hanqi Guo

School of Computer Science
Fudan university
Shanghai, China
hqguo23@m.fudan.edu.cn

Wenqiang Zhang†

Engineering Research Center of
AI&Robotics, Ministry of Education
Academy for
Engineering&Technology
Fudan university
Shanghai, China
wqzhang@fudan.edu.cn

Abstract

Few-shot anomaly detection (FSAD) has emerged as a crucial yet challenging task in industrial inspection, where normal distribution modeling must be accomplished with only a few normal images. While existing approaches typically employ multi-modal foundation models combining language and vision modalities for prompt-guided anomaly detection, these methods often demand sophisticated prompt engineering and extensive manual tuning. In this paper, we demonstrate that a straightforward nearest-neighbor search framework can surpass state-of-the-art performance in both single-class and multi-class FSAD scenarios. Our proposed method, VisionAD, consists of four simple yet essential components: (1) scalable vision foundation models that extract universal and discriminative features; (2) dual augmentation strategies - support augmentation to enhance feature matching adaptability and query augmentation to address the oversights of single-view prediction; (3) multi-layer feature integration that captures both low-frequency global context and high-frequency local details with minimal computational overhead; and (4) a class-aware visual memory bank enabling efficient one-for-all multi-class detection. Extensive evaluations across MVTec-AD, VisA, and Real-IAD benchmarks demonstrate VisionAD's exceptional performance. Using only 1 normal images as support, our method achieves remarkable image-level AUROC scores of 97.4%, 94.8%, and 70.8% respectively, outperforming current state-of-the-art approaches by significant margins (+1.6%, +3.2%, and +1.4%). The training-free nature and superior few-shot

capabilities of VisionAD make it particularly appealing for real-world applications where samples are scarce or expensive to obtain. Code is available at github.com/Qiqigeww/VisionAD.

CCS Concepts

- Computing methodologies → Visual inspection; Anomaly detection.

Keywords

Anomaly detection, Few-shot Learning, Feature Representation, Vision Foundation

1 Introduction

Anomaly Detection (AD) is a critical task aimed at identifying anomalous samples in images that deviate from established normal patterns, with broad applications in fields such as industrial defect detection [36] and medical disease diagnosis [13]. Due to the unpredictability and scarcity of anomalies, along with inherent difficulties in collecting and annotating anomalous samples in real-world scenarios, traditional AD methods typically adopt an unsupervised paradigm, training only on accessible normal samples. However, obtaining sufficient normal samples can still be challenging, especially in scenarios such as the initial manufacturing stages of new products or situations where sample collection itself is difficult. As such, Few-Shot Anomaly Detection (FSAD) has been proposed to reduce annotation costs and novel anomaly detection issues, which holds significant promise for practical applications.

FSAD aims at localizing anomalous regions within a query image by leveraging a few normal support images belonging to the same

*These authors contributed equally to this work.

†Corresponding author

object category. Recently, inspired by the remarkable zero-shot classification capabilities exhibited by vision-language foundation models, particularly CLIP [29], WinCLIP [19] and subsequent studies [2, 44] have been proposed to exploit CLIP’s powerful representation abilities to enhance the performance of low-shot anomaly detection models. Most existing methods fuse prompt-guided and vision-guided anomaly detection branches to obtain the final anomaly score. The vision-guided branch typically stores the nominal patch features into a visual memory bank, detecting anomalies in test samples based on high feature distances to their closest counterparts stored in memory. On the other hand, the prompt-guided anomaly detection branch generates anomaly maps by performing matrix operations between text and image features. For the text, numerous artificial prompts are usually manually designed [32] and/or learned [20], subsequently aggregated to yield normal or abnormal textual features. However, since the aforementioned process relies heavily on meticulous manual designs and/or partial learning strategies, it is burdensome, struggles to generalize to unseen anomalies, and requires bespoke model weights for each dataset category—known as the “one-category-one-model” paradigm (see Fig. 1(a)). For the query image, as CLIP inherently struggles to capture fine-grained local features, existing methods typically resort to simple adapters [4, 11] that map image features to the joint embedding space for comparison with textual features. Alternatively, Li et al. [21] employ a V-V attention mechanism to preserve local information within the CLIP token representations. Considering these intrinsic limitations of the CLIP-based model for FSAD, we are motivated to explore a plain yet effective, training-free approach that solely relies on vision-guided anomaly detection and can generalize across various classes, referred to as the “one-for-all” paradigm.

Inspired by the observation that few-shot anomaly detection is feasible for human annotators relying solely on visual features, we propose a visual-only approach, VisionAD, which performs nearest neighbor searches based on vision foundation models and a visual memory bank. VisionAD can handle various types of product anomalies without requiring domain-specific training data. Instead, it only needs a few normal samples from the target category during the testing phase to perform anomaly detection. Due to its simplicity and effectiveness, VisionAD can be easily deployed in industrial scenarios, as illustrated in Figure 1(b).

Specifically, VisionAD introduces three straightforward yet crucial elements to address the critical issue of limited support data, which typically leads to insufficient patch representations, without increasing complexity or computational burden. First, intuitively, increasing the diversity of support data through simple data augmentation strategies can enhance the adaptability of feature matching. Augmentations, such as multiple rotations and flips applied to support images, can further align the shape and orientation of anomalies—crucial for performance but largely overlooked in previous studies. In addition to increasing the number of support samples, we propose to leverage the consistency and complementarity provided by pseudo multi-view data (i.e., different views of the same object are semantically consistent yet complementary) to mitigate potential oversights of details and interference from irrelevant local features caused by single-view predictions. Second, previous methods typically compare features from different layers separately and then fuse them, causing information isolation among

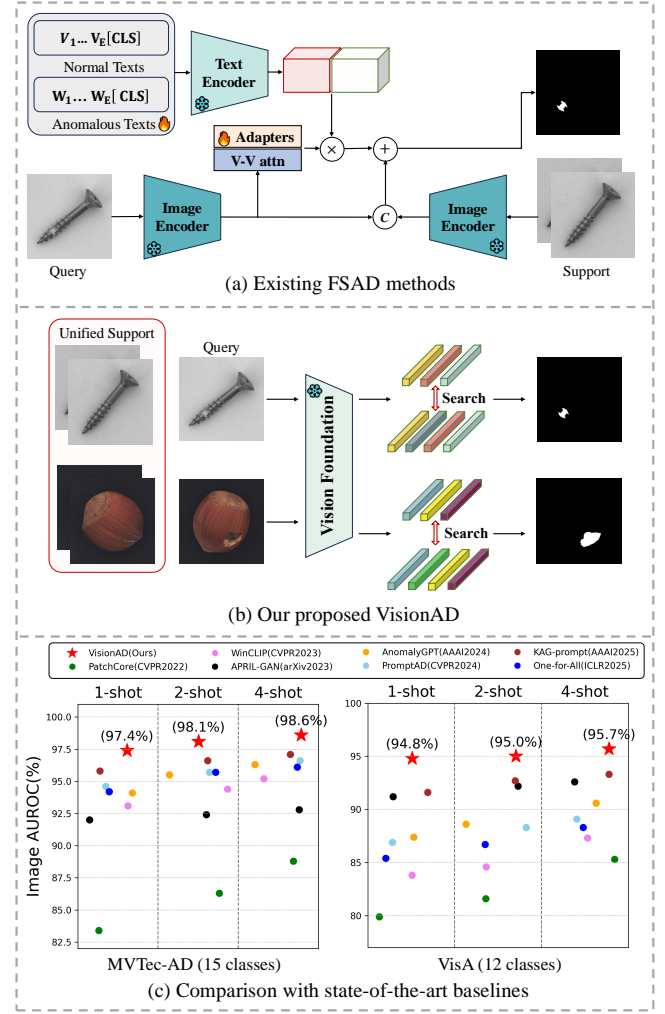


Figure 1: Comparisons between VisionAD and existing FSAD methods. (a) Existing FSAD models rely on complex manual or learnable text prompts and simple adapters or V-V attention for local features, resulting in a cumbersome “one-category-one-model” paradigm. (b) Our VisionAD, a plain, training-free vision-guided approach, generalizes effectively across multiple classes (“one-for-all” paradigm). (c) Comparison with previous SoTA methods on MVtec-AD [1] and VisA [45] across various settings, such as 1-shot, 2-shot, and 4-shot support images.

layers. In contrast, we propose a multi-level feature fusion strategy that integrates intermediate-layer features to jointly capture long-range low-frequency and short-range high-frequency information before performing comparisons, thus effectively enhancing cross-scale feature interactions while minimizing bias towards ImageNet classes. Third, a class-aware visual memory bank is adopted within the one-for-all paradigm by leveraging the similarity between the class tokens of the test image and stored ones.

Extensive experimental results on the MVTec, VisA, and Real-IAD datasets show that the proposed VisionAD achieves unprecedented image-level AUROC scores of 97.4%, 94.8%, and 70.8% under the 1-shot setting, respectively, surpassing previous state-of-the-art methods by a large margin, as illustrated in Figure 1(c).

Our contributions are summarized as follows.

- We propose VisionAD, a plain yet effective vision-only framework for FSAD that operates without complex prompt engineering or dataset-specific training, demonstrating that sophisticated language-vision fusion is not necessary for achieving superior performance in FSAD.
- We introduce three crucial components to address the limited support data challenge: dual augmentation strategy that combines support augmentation and pseudo multi-view transformation, multi-level feature fusion for capturing both global and local information, and class-aware visual memory banks enabling efficient one-for-all detection across categories.
- We conduct comprehensive experiments on popular benchmarks, demonstrating that VisionAD achieves state-of-the-art performance in few-shot anomaly detection, establishing its effectiveness and generalizability across various product categories and datasets.

2 Related Works

Few-shot anomaly detection is designed for scenarios where only a limited amount of normal data is available for training. In this case, normal samples may not fully capture the variability of normality. Many current studies focus on addressing this challenge and can be classified into two categories: CLIP-based (prompt-guided) FSAD and feature-matching-based (vision-guided) FSAD.

CLIP-based FSAD. Since CLIP [29] has demonstrated remarkable performance in zero-shot and few-shot classification, it has gained significant attention and is widely studied for its potential application in anomaly detection. CLIP not only provides descriptive visual embeddings but also computes the similarity between text prompts and test images, as seen in works [4, 11, 19, 20, 25, 32]. WinCLIP [19] designs manual text prompts for both normal and anomalous cases, utilizing sliding windows to extract and aggregate multiscale patch-based votes. APRIL-GAN [4] uses additional linear layers to align patch-level image features with textual features in order to generate anomaly maps. AnomalyGPT[11] generates training data by simulating anomalous images and producing corresponding textual descriptions for each image. PromptAD [20] constructs a large number of negative samples through semantic concatenation. Additionally, it introduces the explicit abnormal edges module to control the margin between normal prompt features and anomaly prompt features. KAG-prompt [32] proposes a kernel-aware hierarchical graph to capture cross-layer contextual information, leading to more accurate anomaly prediction. One-for-All [25] learns a class-shared prompt generator to adaptively generate suitable prompts for each instance. In addition, it proposes a category-aware memory bank to retrieve valid similar features under the one-for-all paradigm. However, these methods either require elaborate prompt engineering or fine-tuning of the prompt embeddings.

Feature-matching-based FSAD. Patch feature matching research is based on the underlying idea of comparing the patch features of test samples with those of normal samples to compute anomaly scores [6, 8, 12, 24, 31]. UniVAD [12] employs the Contextual Component Clustering (C3) module, Component-Aware Patch Matching (CAPM), and Graph-Enhanced Component Modeling (GECM) modules to detect anomalies at different semantic levels and across various domains. INP-Former [24] extracts intrinsic normal prototypes directly from the test image and guides the Decoder to reconstruct only normal tokens, with reconstruction errors serving as anomaly scores. PatchCore [31] uses a maximally representative memory bank of nominal patch features to detect and segment anomalous data at test time. SPADE [6] relies on the K nearest neighbors of pixel-level feature pyramids to detect and segment anomalies within images. PaDiM [8] uses a pretrained convolutional neural network for patch embedding and multivariate Gaussian distributions to obtain a probabilistic representation of the normal class. However, these approaches are not designed for few-shot settings and lack simplicity and generality, so their performance may not meet the demands of manufacturing.

In this research, instead of using category tokens extracted from the Q-Former [25], we leverage class token similarity to retrieve target patch features. Additionally, we propose a straightforward nearest-neighbor search framework, driven by advanced vision foundations, that can efficiently perform anomaly detection with a limited amount of data, thereby meeting the demands of manufacturing.

3 Method

Given an FSAD dataset containing N classes $C = \{C_1, C_2, \dots, C_N\}$, the general few-shot anomaly detection setting typically selects only one class C_i (where $i = 1, 2, \dots, N$ indicates the class number), using the one-category-one-model set $\chi_i = \{(x_{i,\text{normal}}^{\text{Reference}}, (x_{i,\text{normal}}^{\text{Test}}, x_{i,\text{anomaly}}^{\text{Test}})\}$. In contrast, a more practical one-for-all setting encompasses all classes C , covering the all-class sets $\chi = \sum_{i=1}^N \chi_i$ within one unified model. It should be noted that under both settings, each class contains at most K examples, with K typically taking values of 1, 2, or 4. In this paper, we focus on leveraging the reference dataset C to detect and localize anomalies across various categories under the one-for-all paradigm.

3.1 VisionAD Framework

Since language-guided approaches require elaborate designs for training and often struggle to capture fine-grained local features, certain defects can only be detected via visual reference. For instance, "Metal Nut" in MVTecAD has an anomaly type labeled as "flipped upside-down," which can only be identified relatively from a normal image. Therefore, we propose VisionAD, a purely vision-based patch-matching framework that leverages vision foundation models and effective feature fusion to construct a memory bank M . This memory bank stores informative patch-level feature maps of nominal samples at multiple semantic scales. Then, we apply data augmentation to expand the memory bank and better align it with test samples. Identical augmentations are simultaneously applied to both query and reference images to obtain more informative multi-view anomaly scores. Additionally, we introduce a

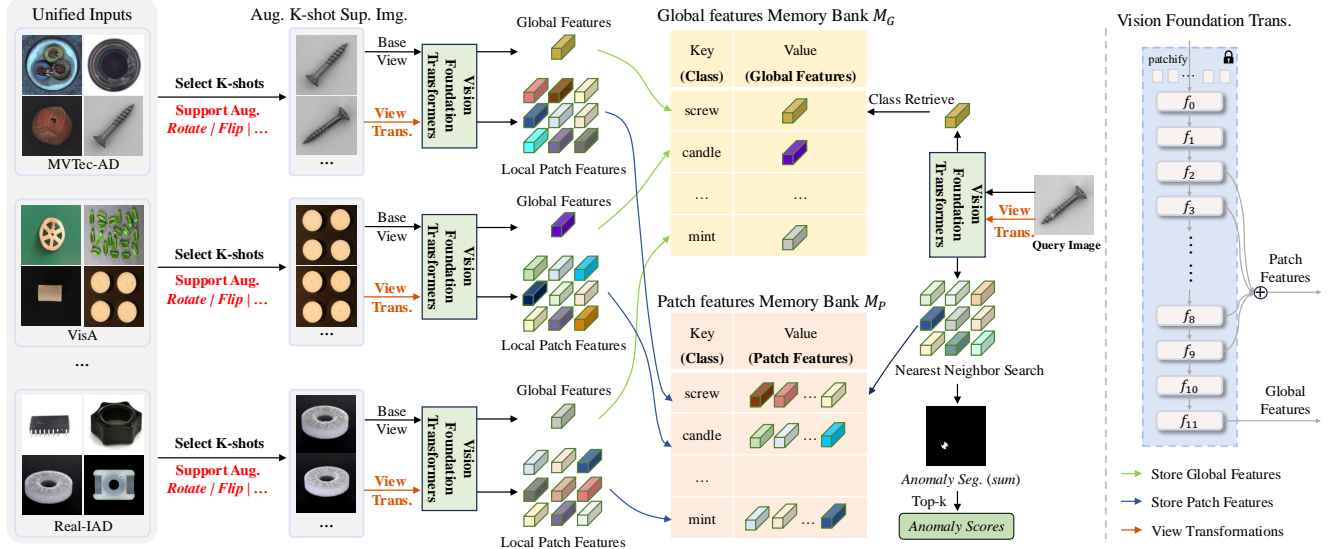


Figure 2: The overall framework of VisionAD. First, the selected k-shots of normal images in the support set are augmented, and an identical view transformation is applied to both the query and all support images (including augmented images). Next, patch features and global features for the reference normal images are extracted using a vision foundation model. These features are then stored in the global memory bank and patch memory bank, respectively. Meanwhile, the features and corresponding categories are combined into key-value pairs. During the testing stage, the category of the image is determined, and the scores from the base view and transformed views are fused to generate the anomaly detection and localization results in the designated patch memory bank.

class-aware memory bank to retrieve category-specific support images, facilitating more precise anomaly detection under one-for-all setting. The overall framework of our method is illustrated in Figure 2.

Vision Foundation Transformers. In order to extract rich features for both normal and anomalous samples, we adopt advanced visual foundation models—particularly ViT architectures pretrained on large-scale datasets [22]. These models typically leverage contrastive learning (e.g., MoCov3 [5], DINO [3]), masked image modeling (e.g., MAE [17], SimMIM [37], BEiT [27]), or their combinations (e.g., iBOT [43], DINOv2 [26]), efficiently capturing both semantic and fine-grained information to generate universal and discriminative features. Specifically, we apply a general-purpose feature extractor F to the input image x_i , generating a feature map of dimensions $H_f \times W_f \times D_f$. To fully harness the benefits of pre-trained models and enable precise differentiation between normal and anomalous samples, we freeze the parameters of F throughout the anomaly detection process, thereby preventing gradient back-propagation.

Recent studies have shown that pre-trained models, whether supervised or self-supervised, tend to generate robust and universal features for anomaly detection tasks. In this paper, we examine the scaling behaviors of VisionAD by systematically analyzing Vision foundational Transformers. Our comprehensive evaluation investigates various aspects, including pre-training strategies (Figure 6) and model sizes (Table 4), as detailed in Section 4.5. Striking

a balance between detection performance and computational efficiency, we adopt the ViT-Large/14 model pretrained using DINOv2-Register [7] as the default extractor.

3.2 Feature Fusion

Inspired by WinCLIP, most vision-language FSAD models employ a vision-guided search branch that stores multi-layer patch embeddings in memory, compares corresponding layers between memory and query images, and aggregates the resulting anomaly maps into a final prediction [4, 19, 44] (Figure 4(a)). Intuitively, comparing more feature pairs allows the FSAD model to exploit richer information across layers for anomaly discrimination. However, due to misalignment between the query and support images, the similarity scores among low-level normal features tend to be underestimated, while high-level features—lacking localized nominal information and overly biased toward the pre-training dataset—yield skewed similarity scores [31]. These discrepancies obscure the true discrepancy between local anomalous features and the memory representations. Utilizing local neighbourhood aggregation (e.g., PatchCore [31] stores multiple intermediate patch-level features) enhances robustness to small spatial deviations without sacrificing spatial resolution (Figure 4(b)). However, feature maps from ResNet-like [18] architectures have limited receptive fields and struggle to capture long-range correlations among distant positions. Given the top-to-bottom consistency of columnar Transformer layers, we propose aggregating all feature maps of interest into a single group rather than enforcing strict layer-to-layer comparisons (Figure 4(c)). This strategy leverages richer, more diversified features for search

and comparison, enabling the detection of subtle local anomalies. Furthermore, since shallow layer features contain low-level visual characteristics critical for precise localization, we further partition the features into low-semantic-level and high-semantic-level groups (Figure 4(d)).

3.3 Support Aug. and Pseudo Multi-View

Support Augmentation. A major challenge faced by FASD is the scarcity of normal samples in the support set, often with fewer than 8 samples available. This results in the difficulty of storing normal features in memory that adequately cover the query features. Previous studies, such as UniVAD [12] and One-for-All [25], have focused on improving the accuracy of feature matching; however, the low matching quality is often caused by misalignment between the query and support images. A direct solution to this issue is to increase the diversity of the support data. We observe that most industrial images under certain categories are highly similar and can be transformed into one another through simple data augmentation, such as rotation, translation, and flipping, as demonstrated by the screw in the Figure 3. Consequently, our natural inclination is to acquire additional data through augmentation strategies like rotation and flipping. This allows the feature memory bank to store more useful features.

Pseudo Multi-View. We find that single-view predictions may overlook important details and focus on trivial features. Drawing inspiration from the complementarity and consistency inherent in multi-view data, we propose a novel approach that simultaneously transforms both query and support images through identical projections. This technique enables the extraction of both shared semantic information and view-specific features, leading to more robust and accurate predictions. The "view" represents not only the camera-shooting perspective, but also the distinct representations of the same sample in multi-view learning [38]. Specifically, we find that simple projection methods, such as image thresholding and flipping (followed by anomaly map inversion), yield substantial performance improvements, as illustrated in Figure 3. These transformations can simulate different viewing conditions: thresholding mimics camera parameter adjustments, while flipping emulates alternative viewing angles.

3.4 Category-Indexed Memory Bank

Under the one-for-all paradigm, mixing patch features from multiple categories within a single memory bank can complicate the nearest neighbor search and increase computation time. Additionally, regional similarities between images from different categories may lead to undesired feature matching. To address these issues, patch features $\mathbf{P}(\mathbf{F}(x_i))$ extracted from normal image x_i in the support set are stored in a dedicated patch feature memory bank \mathbf{M}_P , where they are paired with the corresponding category label C_i . Similarly, global features \mathbf{G}_i extracted from normal image x_i in the support set are stored in a separate global feature memory bank \mathbf{M}_G , with key-value pairs formed based on their category C_i .

The category-indexed patch and global feature memory banks \mathbf{M}_P and \mathbf{M}_G are defined as:

$$\mathbf{M}_P = \{\{C_1; \mathbf{P}(\mathbf{F}(x_1))\}, \dots, \{C_N; \mathbf{P}(\mathbf{F}(x_N))\}\} \quad (1)$$

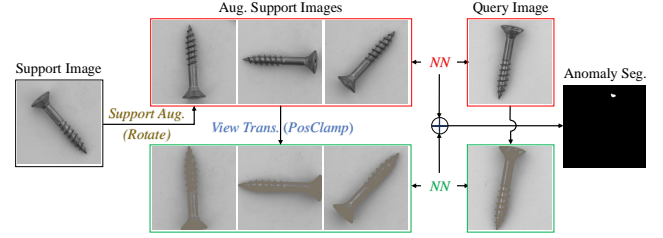


Figure 3: Support Enhancement and Pseudo Multi-View for Anomaly Detection.

$$\mathbf{M}_G = \{\{C_1; \mathbf{G}(\mathbf{F}(x_1))\}, \dots, \{C_N; \mathbf{G}(\mathbf{F}(x_N))\}\} \quad (2)$$

During the testing phase, the category of the test image is first retrieved by measuring the similarity between the class token G_s of the test image and the stored tokens. The corresponding patch features can then be retrieved through the category, enabling anomaly detection and localization, as shown in Figure 2. The pseudo-code for establishing both the patch feature memory bank and the global feature memory bank is provided in Algorithm 2.

3.5 Anomaly Detection and Segmentation

First, we randomly select one sample from the k-shot normal samples of each class and construct a global feature memory bank, storing them as key-value pairs based on their respective categories (Equation (2)). Then, we expand the support set using augmentation strategies such as rotation and flipping. Their patch features are extracted using a vision foundation model and stored in the patch feature memory bank (Equation (1)).

In the testing phase, we first determine the category of the test image by measuring the distance between its class token and those stored in \mathbf{M}_G . The category corresponding to the global feature with the smallest distance is then selected as the category of the test image:

$$C = \min \mathcal{D} \left(G \left(F(x^{\text{test}}) \right), \mathbf{M}_G \right) \quad (3)$$

Then, the localization result $Score_{pix_ori}$ is obtained by calculating the distance between the query patch and the most similar corresponding patch in \mathbf{M}_P :

$$Score_{pix_ori} = \text{Up} \left(1 - \max_{m_j \in \mathbf{M}_P} \left(\mathbf{P}_i \left(\mathbf{F}(x^{\text{test}}) \right) \cdot m_j \right) \right) \quad (4)$$

Similarly, identical view transformation is applied to both the query and all reference images (including augmented ones) to obtain the localization result $Score_{pix_view}$.

The final result of anomaly localization is:

$$Score_{pix} = Score_{pix_ori} + Score_{pix_view} \quad (5)$$

For image-level anomaly score, to retain potentially important information beyond the global maximum, we use the average of the top- k highest values (top 1% pixels in an anomaly map) in the prediction map as our metric. This strategy effectively aggregates multiple significant anomaly signals present in the prediction map. The image-level anomaly score is:

$$Score_{img} = \text{Mean}(\text{Top}-k(Score_{pix})) \quad (6)$$

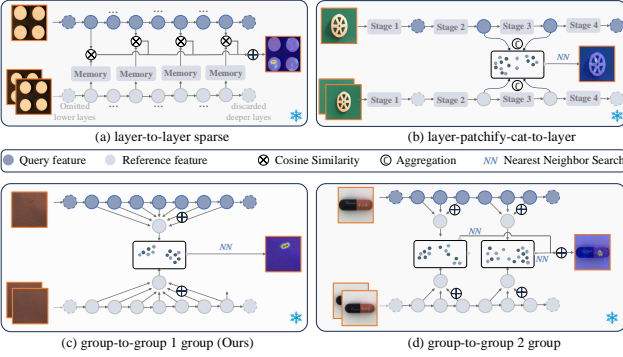


Figure 4: Schemes of Feature Fusion. (a) Layer-to-layer (sparse). (b) layer-patchify-cat-to-layer. (c) group-to-group, 1-group (Ours). (d) group-to-group, 2-group.

4 Experiments

4.1 Experimental Settings

Datasets. MVTec-AD [1] consists of 15 object categories, including 5 texture classes and 10 object classes, with 3,629 normal images in the training set and 1,725 images in the test set (467 normal and 1,258 anomalous). VisA [45] contains 12 object categories. With the official data split, the training set includes 8,659 normal images, and the test set includes 2,162 images (962 normal and 1,200 anomalous). Real-IAD [35] is a large-scale, recently released dataset for unsupervised anomaly detection, covering 30 distinct object categories. The official split, which includes all views, results in 36,465 normal images in the training set and 114,585 images in the test set (63,256 normal and 51,329 anomalous).

Metrics. Consistent with prior studies [14, 40], we evaluate anomaly detection and localization using metrics such as the Area Under the Receiver Operating Characteristic Curve (AUROC). Additionally, we employ the Area Under the Precision-Recall Curve (AUPR) for anomaly detection and the Per-Region Overlap (PRO) for anomaly localization to provide a more comprehensive analysis of the model’s performance.

Implementation Details. In the few-normal-shot setting, no further training is performed on the anomaly detection datasets for VisionAD. By default, we use the ViT-Base/14 (patch size = 14) pre-trained by DINOv2-R [7] as our image encoder, with its parameters frozen. The input image is first resized to 448^2 and then center-cropped to 392^2 , ensuring the feature map (28^2) is sufficiently large for anomaly localization. As previously mentioned, we utilize the middle 8 layers of the 12-layer ViT-Base for feature fusion. ViT-Small, which also has 12 layers, follows the same selection. ViT-Large, with 24 layers, uses layers [4,6,8,...,19] for fusion (with indexing starting from 0).

4.2 Comparisons with State-of-the-Arts

Table 1 and Table 2 demonstrate the comparison results of VisionAD (ViT-Large) with existing few-shot anomaly detection methods [4, 6, 8, 11, 19, 20, 24, 25, 31, 32]. VisionAD shows significant improvements over all methods across the MVTec, VisA, and Real-IAD datasets in almost all metrics. On the widely used

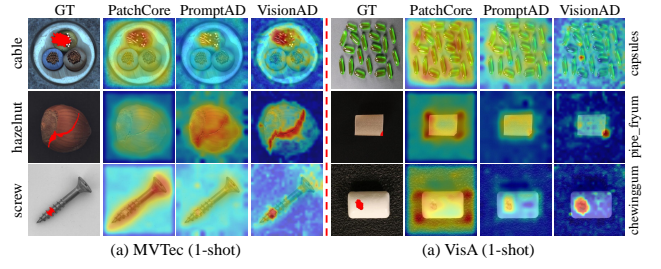


Figure 5: Qualitative comparison results of 1-shot pixel-level anomaly detection on MVTec [1] and VisA [45].

MVTec-AD dataset, VisionAD achieves AUROC/AUPR/PRO performance of 97.4/99.0/92.5 (%), outperforming the previous state-of-the-art (SoTA) methods by 1.6/0.9/1.7, respectively, in the 1-shot setting compared to the suboptimal method results. On the popular VisA dataset, VisionAD achieves AUROC/AUPR/pAUROC/PRO performance of 94.8/95.0/97.6/91.6, surpassing previous SoTAs by 3.2/1.7/0.6/1.6. On the Real-IAD dataset, which contains 30 classes with 5 camera views each, VisionAD produces AUROC/AUPR/pAUROC/PRO performance of 70.8/66.7/95.7/84.9, outperforming previous SoTAs by 1.4/3.6/0.8/3.1, demonstrating its scalability to highly complex scenarios. Averaging the results across all metrics, VisionAD shows the best performance. Furthermore, VisionAD achieves competitive results in the pAUROC metric on MVTec and state-of-the-art performance in the 2-shot and 4-shot settings. The quantitative results of VisionAD in anomaly localization highlight its significant advantages in performance under different numbers of support images.

4.3 Visualization Results

Fig. 5 shows the partial visualization results of VisionAD on MVTec and VisA dataset. Compared to PatchCore [31] and WinCLIP [19], VisionAD produces more distinctive and precise anomaly maps in the 1-shot setting. Additionally, VisionAD is capable of accurately locating subtle anomalies that are often overlooked. This robustness and reliability under few-shot settings underscore the potential practical applicability of VisionAD in real-world scenarios. For more qualitative results refer to Appendix C.

4.4 Compared With Multi-class Full-Shot Methods

In Table 3, we present the comparison results of VisionAD under few-shot settings with several prior works evaluated under the full-shot multi-class setting on the MVTec and VisA datasets. It can be observed that, compared to some methods under the full-shot setting, VisionAD achieves better image-level results and competitive pixel-level results. This fully demonstrates the strong ability of VisionAD in few-shot settings. Additionally, VisionAD outperforms early full-shot AD methods such as UniAD [39], SimpleNet [23], DeSTSeg [41], and DiAD [16], although there remains a gap between VisionAD and the latest full-shot one-for-all methods, including MambaAD [15] and Dinomaly [14]. This highlights the effectiveness of our method in leveraging limited data.

Table 1: Performance comparisons of the FSAD methods on the MVTecAD and VisA datasets across different few-shot settings. We report the mean and standard deviation over 5 random seeds for each measurement. Bold indicates the best performance and underlining indicates sub-optimal results.

Setup	Method	Public	MVTecAD				VisA				avg
			AUROC	AUPR	pAUROC	PRO	AUROC	AUPR	pAUROC	PRO	
1-shot	PatchCore [31]	CVPR2022	83.4	92.2	92.0	79.7	79.9	82.8	95.4	80.5	85.7
	WinCLIP [19]	CVPR2023	93.1	96.5	95.2	87.1	83.8	85.1	96.4	85.1	90.3
	APRIL-GAN [4]	arXiv2023	92.0	95.8	95.1	90.6	91.2	<u>93.3</u>	96.0	<u>90.0</u>	93.0
	AnomalyGPT [11]	AAAI2024	94.1	95.9	95.3	89.5	87.4	88.7	96.2	82.9	91.3
	PromptAD [20]	CVPR2024	94.6	97.1	95.9	87.9	86.9	88.4	96.7	85.1	91.6
	KAG-prompt [32]	AAAI2025	<u>95.8</u>	<u>98.1</u>	96.2	<u>90.8</u>	<u>91.6</u>	93.2	<u>97.0</u>	85.2	<u>93.5</u>
	One-for-All [25]	ICLR2025	94.2	97.2	96.4	89.8	85.4	87.5	96.9	87.3	91.8
	VisionAD (ours)	-	97.4±0.4	99.0±0.2	<u>96.2±0.2</u>	92.5±0.3	94.8±1.0	95.0±0.9	97.6±0.3	91.6±0.8	95.5
2-shot	PatchCore [31]	CVPR2022	86.3	93.8	93.3	82.3	81.6	84.8	96.1	82.6	87.6
	WinCLIP [19]	CVPR2023	94.4	97.0	96.0	88.4	84.6	85.8	96.8	86.2	91.1
	APRIL-GAN [4]	arXiv2023	92.4	96.0	95.5	<u>91.3</u>	92.2	<u>94.2</u>	96.2	<u>90.1</u>	93.5
	AnomalyGPT [11]	AAAI2024	95.5	96.8	95.6	90.0	88.6	89.0	96.4	83.4	91.9
	PromptAD [32]	CVPR2024	95.7	97.9	96.2	88.5	88.3	90.0	97.1	85.8	92.4
	KAG-prompt [32]	AAAI2025	<u>96.6</u>	<u>98.5</u>	96.5	91.1	<u>92.7</u>	<u>94.2</u>	<u>97.4</u>	86.7	<u>94.2</u>
	One-for-All [25]	ICLR2025	95.7	97.9	96.7	90.3	86.7	88.6	97.2	87.9	92.6
	VisionAD (ours)	-	98.1±0.3	99.3±0.1	<u>96.6±0.1</u>	93.2±0.2	95.0±0.3	95.2±0.6	97.7±0.0	91.8±0.3	95.9
4-shot	PatchCore [31]	CVPR2022	88.8	94.5	94.3	84.3	85.3	87.5	96.8	84.9	89.6
	WinCLIP [19]	CVPR2023	95.2	97.3	96.2	89.0	87.3	88.8	97.2	87.6	92.3
	APRIL-GAN [4]	arXiv2023	92.8	96.3	95.9	<u>91.8</u>	92.6	94.5	96.2	<u>90.2</u>	93.8
	AnomalyGPT [11]	AAAI2024	96.3	97.6	96.2	90.7	90.6	91.3	96.7	84.6	93.0
	PromptAD [32]	CVPR2024	96.6	98.5	96.5	90.5	89.1	90.8	97.4	86.2	93.2
	KAG-prompt [32]	AAAI2025	<u>97.1</u>	<u>98.8</u>	96.7	91.4	<u>93.3</u>	<u>94.6</u>	97.7	87.6	<u>94.7</u>
	One-for-All [25]	ICLR2025	96.1	98.1	97.0	91.2	88.3	89.6	97.4	88.3	93.2
	VisionAD (ours)	-	98.6±0.1	99.5±0.1	<u>96.9±0.1</u>	93.7±0.1	95.7±0.3	95.9±0.3	98.0±0.0	92.5±0.2	96.4

4.5 Ablation Study

Overall Ablation. We conduct experiments to verify the effectiveness of different modules: Advanced Foundation (AF), Feature Fusion (FF), Support Augmentation (SA), Pseudo Multi-View Transformation (PMVT), and Category-Indexed Memory Bank (CIMB). Image-level and pixel-level results on MVTec-AD and VisA under the 1-shot setting are shown in Table 5. In the first row, we provide a baseline model without incorporating any of the proposed modules, using the common DINO, the last layer feature, no augmentation, and no category-indexed memory bank. Each module contributes to the superior anomaly classification performance of VisionAD. A slight improvement is observed in anomaly segmentation due to the subtle anomaly areas. The combined use of all modules helps the model search more accurately. When applying VisionAD to multi-class FSAD scenarios, the use of the Category-Indexed Memory Bank does not result in any performance degradation, as the semantic differences in images are often quite clear. More ablation and detailed experiment results refer to Appendix A and B.

ViT Foundations. We conduct extensive experiments to explore the impact of diverse pre-trained ViT-Base foundations, including

DeiT [34], MAE [17], D-iGPT [30], MOCOv3 [5], DINO [3], iBot [43], DINoV2 [26], Proteus [42], SynCLR [33], and DINoV2-R [7]. As shown in Figure 6, compared to the less affected anomaly segmentation, anomaly classification performance shows a more pronounced difference. However, some foundation models can produce competitive results, with image-level/pixel-level AUROC exceeding 90%/95%. MAE has exceptionally low AUROC, which has been reported to be less effective across various unsupervised tasks (e.g., kNN and linear-probing) without fine-tuning [26]. The optimal input size varies because these foundations are pre-trained on different resolutions. Interestingly, we found that anomaly detection performance is strongly correlated with the accuracy of ImageNet linear-probing (freezing the backbone and only tuning the linear classifier) of the foundation model, suggesting that future improvements could be achieved by simply adopting a more advanced foundation model.

Additionally, we found that the performance of the proposed VisionAD benefits from scaling, as shown in Table 4. ViT-Large

Table 2: Performance comparisons of the FSAD methods on the Real-IAD datasets across different few-shot settings.

Setup	Method	Public	Real-IAD				avg
			AUROC	AUPR	pAUROC	PRO	
1-shot	SPADE [6]	arXiv2020	51.2	45.6	59.5	19.3	43.9
	PaDiM [8]	ICPR2020	52.9	47.4	84.9	52.7	59.5
	PatchCore [31]	CVPR2022	59.3	55.8	89.6	60.5	66.3
	WinCLIP [19]	CVPR2023	69.4	56.8	91.9	71.0	72.3
	PromptAD [20]	CVPR2024	52.2	41.6	84.9	58.4	59.3
	INP-Former [24]	CVPR2025	67.5	63.1	94.9	81.8	76.8
VisionAD (ours)			-	70.8±1.2	66.7±1.5	95.7±0.3	84.9±0.7
2-shot	SPADE [6]	arXiv2020	50.9	45.5	59.5	19.2	43.8
	PaDiM [8]	ICPR2020	55.9	49.6	88.5	61.6	63.9
	PatchCore [31]	CVPR2022	63.3	59.7	92.0	66.1	70.3
	WinCLIP [19]	CVPR2023	70.9	58.7	93.2	74.7	74.4
	PromptAD [20]	CVPR2024	57.7	41.1	86.4	61.0	61.6
	INP-Former [24]	CVPR2025	70.6	66.1	96.0	83.8	79.1
VisionAD (ours)			-	74.7±1.2	70.1±1.7	96.4±0.3	86.5±1.1
4-shot	SPADE [6]	arXiv2020	50.8	45.8	59.5	19.2	43.8
	PaDiM [8]	ICPR2020	60.3	53.5	90.9	67.6	68.1
	PatchCore [31]	CVPR2022	66.0	62.2	92.9	68.6	72.4
	WinCLIP [19]	CVPR2023	73.0	61.8	93.8	76.4	76.2
	PromptAD [20]	CVPR2024	59.7	43.5	86.9	61.9	63.0
	INP-Former [24]	CVPR2025	76.7	72.3	97.3	89.0	83.8
VisionAD (ours)			-	79.1±2.1	74.7±2.3	97.3±0.3	88.9±1.4
8-shot			-	80.9±1.2	78.1±1.7	97.3±0.3	89.1±1.4
VisionAD (ours)			-	80.9±1.2	78.1±1.7	97.3±0.3	89.1±1.4

Table 3: Performance comparisons under full-shot multi-class(one-for-all) setting. Results below our 1-shot are marked in red, and those below our 8-shot are marked in blue.

Method	Public	Setup	MVtec		VisA	
			AUROC	pAUROC	AUROC	pAUROC
VisionAD (Ours)	-	1-shot	97.4±0.4	96.2±0.2	94.8±1.0	97.6±0.3
		2-shot	98.1±0.3	96.6±0.1	95.0±0.3	97.7±0.0
		4-shot	98.6±0.1	96.9±0.1	95.7±0.3	98.0±0.0
		8-shot	98.9±0.2	97.1±0.1	96.3±0.3	98.2±0.0
UniAD [39]	NeurIPS2022		96.5	96.8	91.9	98.6
SimpleNet [23]	CVPR2023		95.3	96.9	87.2	96.8
DeSTSeg [41]	CVPR2023		89.2	93.1	88.9	96.1
DiAD [16]	AAAI2024 full-shot		97.2	96.8	86.8	96.0
MambaAD [15]	NeurIPS2024		98.6	97.7	94.3	98.5
ViTAD [40]	CVIU2025		98.3	97.7	90.5	98.2
Dinomaly [14]	CVPR2025		99.6	98.4	98.7	98.7

Table 4: Scaling of ViT model sizes on MVtec and VisA under 1-shot setting (%). Im/s (Throughput, image per second) is measured on NVIDIA RTX4090 with batch size=8. †:default.

Arch.	Params	MACs	Im/s	MVtec		VisA	
				AUROC	pAUROC	AUROC	pAUROC
ViT-Small	18.0M	14.2G	52.0	96.3	95.6	91.3	96.8
ViT-Base	71.3M	56.2G	26.6	97.6	96.0	92.7	97.2
ViT-Large†	239.9M	189.2G	10.1	97.7	96.2	93.7	97.3

further boosts VisionAD to an unprecedented level. This scalability allows users to select an appropriate model size based on the computational resources available in their specific scenario.

Table 5: Ablation study under 1-shot setting (%). AF: Advanced Foundation. FF: Feature Fusion. SA: Support Augmentation. PMVT: Pseudo Multi-View Transformation. CIMB: Category-Indexed Memory Bank. CS: Class-Separated Setting. MC: Multi-Class Setting.

Setting	AF	FF	SA	PMVT	CIMB	MVtec		VisA	
						AUROC	pAUROC	AUROC	pAUROC
CS	✓	✓	✓	✓	✓	89.00	95.17	78.32	95.41
						92.83	94.44	80.50	93.57
						94.96	95.50	86.81	96.24
						97.07	95.57	90.17	96.36
MC	✓	✓	✓	✓	✓	97.60	96.01	92.66	97.22
						97.06	95.33	92.49	97.26

Table 6: Performance using different support augmentations, view transformations under 1-shot setting.

Aug.	MVtec		VisA	
	AUROC	pAUROC	AUROC	pAUROC
Baseline	95.0	95.5	86.8	96.2
Baseline+Rot.†	97.0	95.6	90.2	96.4
Baseline+Rot.+flip	97.1	95.6	90.2	96.4
Baseline+Rot.+flip+affine	97.1	95.7	90.1	96.4
Baseline+PosClamp	95.5	95.9	88.8	97.0
Baseline+NegClamp	94.8	95.4	84.2	96.0
Baseline+XFlip	95.0	95.6	87.0	96.4
Baseline+YFlip	95.3	95.7	87.1	96.4
Baseline+RBSwap	95.0	95.5	86.7	96.3
Baseline+PosClamp+Yflip†	95.5	96.0	89.2	97.1
Baseline+Rot.+PosClamp+Yflip	97.6	96.0	92.7	97.2

Table 7: Performance using different Fuser variants under 1-shot setting (without SA and PMVT). The numbers represent the usage of the corresponding layer features, where the variants, separated by commas, indicate the comparison and subsequent fusion to obtain the anomaly map.

Fuser Variant	MVtec		VisA	
	AUROC	pAUROC	AUROC	pAUROC
12(last layer)	92.8	94.4	80.5	93.6
3,6,9,12	93.8	96.1	87.4	96.0
345678910†	95.0	95.5	86.8	96.2
3456,78910	94.4	95.9	87.2	95.8

Support Augmentation and Pseudo Multi-View Transformation. To validate the effectiveness of our support Augmentation and pseudo multi-view transformation design, we conducted an ablation study using different support augmentations and view transformations. The results are presented in Table 6. The second section shows the performance of gradually adding rotation, flip, and affine transformations to support images. A significant performance improvement occurs when rotating support images, demonstrating

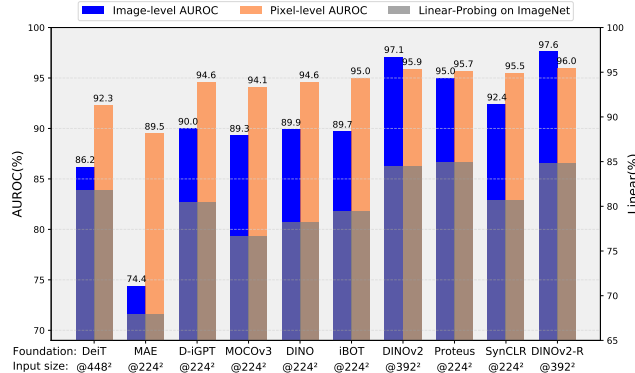


Figure 6: Image-level/pixel-level results on MVTec [1] in the 1-shot setting using various ViT-Base foundations, and their linear-probing accuracy on ImageNet.

that simple augmentation strategies allow the feature memory bank to store more useful and diverse features. The third section shows the performance of applying PositiveClamp, NegativeClamp, XFlip, YFlip, R-B channel swap to query and support images. The performance improvement based on some view transformations indicates that pseudo multi-view enhances the accuracy and robustness of the predictions.

Feature Fusion Variants. As shown in Table 7, we conducted an ablation study to explore the impact of different layer feature fusion on the results. We first aggregate multi-layer feature similarity (Fig. 4 (a) and the first row in Table 7). Then, we employ a single feature group (Fig. 4 (c) and the third row in Table 7), and two feature groups (Fig. 4 (d) and the fourth row in Table 7). The results in the second row show the use of the last layer feature for search. When adopting the structure in Fig. 4 (c) and (d), a significant improvement in AUROC is observed on MVTec, with almost identical performance on VisA. This indicates that our strategy leverages richer, more diversified features for search and comparison, enabling the detection of subtle local anomalies.

5 Conclusion

In this paper, we propose a training-free, vision-guided and minimalistic FSAD framework termed VisionAD which is proposed to address sophisticated prompt engineering and extensive manual tuning of existing methods. We present four key elements in VisionAD, i.e., Foundation Transformer, Dual Augmentation Strategies, Multi-layer Feature Integration, and a class-aware visual memory bank, that can boost the performance under the challenging few-shot setting without fancy modules and tricks. Extensive experiments on MVTec AD, VisA, and Real-IAD demonstrate our superiority over previous state-of-the-art approaches under FSAD setting.

References

- [1] Paul Bergmann, Michael Fauser, David Sattlegger, and Carsten Steger. 2019. MVTec AD—A comprehensive real-world dataset for unsupervised anomaly detection. In *Proceedings of the IEEE/CVF conference on computer vision and pattern recognition*. 9592–9600.
- [2] Yunkang Cao, Jiangning Zhang, Luca Frittoli, Yuqi Cheng, Weiming Shen, and Giacomo Boracchi. 2024. Adaclip: Adapting clip with hybrid learnable prompts for zero-shot anomaly detection. In *European Conference on Computer Vision*. Springer, 55–72.
- [3] Mathilde Caron, Hugo Touvron, Ishan Misra, Hervé Jégou, Julien Mairal, Piotr Bojanowski, and Armand Joulin. 2021. Emerging properties in self-supervised vision transformers. In *Proceedings of the IEEE/CVF international conference on computer vision*. 9650–9660.
- [4] Xuhai Chen, Yue Han, and Jiangning Zhang. 2023. A zero-/few-shot anomaly classification and segmentation method for cvpr 2023 vand workshop challenge tracks 1&2: 1st place on zero-shot ad and 4th place on few-shot ad. *arXiv preprint arXiv:2305.17382* 2, 4 (2023).
- [5] Xinlei Chen, Saining Xie, and Kaiming He. 2021. An empirical study of training self-supervised vision transformers. In *Proceedings of the IEEE/CVF international conference on computer vision*. 9640–9649.
- [6] Niv Cohen and Yedid Hoshen. 2020. Sub-image anomaly detection with deep pyramid correspondences. *arXiv preprint arXiv:2005.02357* (2020).
- [7] Timothée Darcret, Maxime Oquab, Julien Mairal, and Piotr Bojanowski. 2023. Vision transformers need registers. *arXiv preprint arXiv:2309.16588* (2023).
- [8] Thomas Defard, Aleksandr Setkov, Angelique Loesch, and Romaric Audigier. 2021. Padim: a patch distribution modeling framework for anomaly detection and localization. In *International conference on pattern recognition*. Springer, 475–489.
- [9] Jia Deng, Wei Dong, Richard Socher, Li-Jia Li, Kai Li, and Li Fei-Fei. 2009. Imagenet: A large-scale hierarchical image database. In *IEEE Conference on Computer Vision and Pattern Recognition*. 248–255.
- [10] Enrico Fini, Mustafa Shukor, Xujun Li, Philipp Dufter, Michal Klein, David Heldmann, Sai Aitharaju, Victor Guilherme Turrisi da Costa, Louis Béthune, Zhe Gan, et al. 2024. Multimodal autoregressive pre-training of large vision encoders. *arXiv preprint arXiv:2411.14402* (2024).
- [11] Zhaopeng Gu, Bingke Zhu, Guibo Zhu, Yingying Chen, Ming Tang, and Jinqiao Wang. 2024. Anomalygpt: Detecting industrial anomalies using large vision-language models. In *Proceedings of the AAAI conference on artificial intelligence*, Vol. 38. 1932–1940.
- [12] Zhaopeng Gu, Bingke Zhu, Guibo Zhu, Yingying Chen, Ming Tang, and Jinqiao Wang. 2024. UniVAD: A Training-free Unified Model for Few-shot Visual Anomaly Detection. *arXiv preprint arXiv:2412.03342* (2024).
- [13] Jia Guo, Shuai Lu, Lize Jia, Weihang Zhang, and Huiqi Li. 2023. Encoder-decoder contrast for unsupervised anomaly detection in medical images. *IEEE transactions on medical imaging* 43, 3 (2023), 1102–1112.
- [14] Jia Guo, Shuai Lu, Weihang Zhang, Fang Chen, Hongen Liao, and Huiqi Li. 2024. Dinomaly: The Less Is More Philosophy in Multi-Class Unsupervised Anomaly Detection. *arXiv preprint arXiv:2405.14325* (2024).
- [15] Haoyang He, Yuhu Bai, Jiangning Zhang, Qingdong He, Hongxu Chen, Zhenye Gan, Chengjie Wang, Xiangtai Li, Guanzhong Tian, and Lei Xie. 2024. Mambaad: Exploring state space models for multi-class unsupervised anomaly detection. *arXiv preprint arXiv:2404.06564* (2024).
- [16] Haoyang He, Jiangning Zhang, Hongxu Chen, Xuhai Chen, Zhishan Li, Xu Chen, Yabiao Wang, Chengjie Wang, and Lei Xie. 2024. A diffusion-based framework for multi-class anomaly detection. In *Proceedings of the AAAI conference on artificial intelligence*, Vol. 38. 8472–8480.
- [17] Kaiming He, Xinlei Chen, Saining Xie, Yanghao Li, Piotr Dollár, and Ross Girshick. 2022. Masked autoencoders are scalable vision learners. In *Proceedings of the IEEE/CVF conference on computer vision and pattern recognition*. 16000–16009.
- [18] Kaiming He, Xiangyu Zhang, Shaoqing Ren, and Jian Sun. 2016. Deep residual learning for image recognition. In *Proceedings of the IEEE conference on computer vision and pattern recognition*. 770–778.
- [19] Jongheon Jeong, Yang Zou, Taewan Kim, Dongqing Zhang, Avinash Ravichandran, and Onkar Dabeer. 2023. Winclip: Zero-/few-shot anomaly classification and segmentation. In *Proceedings of the IEEE/CVF Conference on Computer Vision and Pattern Recognition*. 19606–19616.
- [20] Yiting Li, Adam Goodige, Faya Liu, and Chuan-Sheng Foo. 2024. Promptpad: Zero-shot anomaly detection using text prompts. In *Proceedings of the IEEE/CVF Winter Conference on Applications of Computer Vision*. 1093–1102.
- [21] Yi Li, Hualiang Wang, Yiqun Duan, and Xiaomeng Li. 2023. Clip surgery for better explainability with enhancement in open-vocabulary tasks. *arXiv e-prints* (2023), arXiv–2304.
- [22] Ze Liu, Yutong Lin, Yue Cao, Han Hu, Yixuan Wei, Zheng Zhang, Stephen Lin, and Baining Guo. 2021. Swin transformer: Hierarchical vision transformer using shifted windows. In *Proceedings of the IEEE/CVF international conference on computer vision*. 10012–10022.
- [23] Zhihang Liu, Yiming Zhou, Yuansheng Xu, and Zilei Wang. 2023. Simplenet: A simple network for image anomaly detection and localization. In *Proceedings of the IEEE/CVF conference on computer vision and pattern recognition*. 20402–20411.
- [24] Wei Luo, Yunkang Cao, Haiming Yao, Xiaotian Zhang, Jianan Lou, Yuqi Cheng, Weiming Shen, and Wenyong Yu. 2025. Exploring Intrinsic Normal Prototypes within a Single Image for Universal Anomaly Detection. *arXiv preprint arXiv:2503.02424* (2025).

- [25] Wenxi Lv, Qinliang Su, and Wenchao Xu. [n. d.]. One-for-All Few-Shot Anomaly Detection via Instance-Induced Prompt Learning. In *The Thirteenth International Conference on Learning Representations*.
- [26] Maxime Oquab, Timothée Darct, Théo Moutakanni, Huy Vo, Marc Szafraniec, Vasil Khalidov, Pierre Fernandez, Daniel Haziza, Francisco Massa, Alaaeldin El-Nouby, et al. 2023. Dinov2: Learning robust visual features without supervision. *arXiv preprint arXiv:2304.07193* (2023).
- [27] Zhiliang Peng, Li Dong, Hangbo Bao, Qixiang Ye, and Furu Wei. 2022. Beit v2: Masked image modeling with vector-quantized visual tokenizers. *arXiv preprint arXiv:2208.06366* (2022).
- [28] Z Peng, L Dong, H Bao, Q Ye, and F Wei. 2022. Beit v2: Masked image modeling with vector-quantized visual tokenizers. *arXiv preprint arXiv:2208.06366* (2022).
- [29] Alec Radford, Jong Wook Kim, Chris Hallacy, Aditya Ramesh, Gabriel Goh, Sandhini Agarwal, Girish Sastry, Amanda Askell, Pamela Mishkin, Jack Clark, et al. 2021. Learning transferable visual models from natural language supervision. In *International conference on machine learning*. PMLR, 8748–8763.
- [30] Sucheng Ren, Zeyu Wang, Hongru Zhu, Junfei Xiao, Alan Yuille, and Cihang Xie. 2023. Rejuvenating image-GPT as Strong Visual Representation Learners. *arXiv preprint arXiv:2312.02147* (2023).
- [31] Karsten Roth, Latha Pemula, Joaquin Zepeda, Bernhard Schölkopf, Thomas Brox, and Peter Gehler. 2022. Towards total recall in industrial anomaly detection. In *Proceedings of the IEEE/CVF conference on computer vision and pattern recognition*. 14318–14328.
- [32] Fenfang Tao, Guo-Sen Xie, Fang Zhao, and Xiangbo Shu. 2024. Kernel-Aware Graph Prompt Learning for Few-Shot Anomaly Detection. *arXiv preprint arXiv:2412.17619* (2024).
- [33] Yonglong Tian, Lijie Fan, Kaifeng Chen, Dina Katabi, Dilip Krishnan, and Phillip Isola. 2024. Learning vision from models rivals learning vision from data. In *Proceedings of the IEEE/CVF conference on computer vision and pattern recognition*. 15887–15898.
- [34] Hugo Touvron, Matthieu Cord, Matthijs Douze, Francisco Massa, Alexandre Sablayrolles, and Hervé Jégou. 2021. Training data-efficient image transformers & distillation through attention. *arXiv preprint arXiv:2012.12877* (2021).
- [35] Chengjie Wang, Wenbing Zhu, Bin-Bin Gao, Zhenyu Gan, Jiangning Zhang, Zhihao Gu, Shuguang Qian, Mingang Chen, and Lizhuang Ma. 2024. Real-iad: A real-world multi-view dataset for benchmarking versatile industrial anomaly detection. In *Proceedings of the IEEE/CVF Conference on Computer Vision and Pattern Recognition*. 22883–22892.
- [36] Qishan Wang, Shuyong Gao, Li Xiong, Aili Liang, Kaidong Jiang, and Wenqiang Zhang. 2024. A Casting Surface Dataset and Benchmark for Subtle and Confusable Defect Detection in Complex Contexts. *IEEE Sensors Journal* 24, 10 (2024), 16721–16733. doi:10.1109/JSEN.2024.3387082
- [37] Zhenda Xie, Zheng Zhang, Yue Cao, Yutong Lin, Jianmin Bao, Zhuliang Yao, Qi Dai, and Han Hu. 2022. Simmim: A simple framework for masked image modeling. In *Proceedings of the IEEE/CVF conference on computer vision and pattern recognition*. 9653–9663.
- [38] Xiaoliang Yan, Shizhe Hu, Yiqiao Mao, Yangdong Ye, and Hui Yu. 2021. Deep multi-view learning methods: A review. *Neurocomputing* 448 (2021), 106–129.
- [39] Zhiyuan You, Lei Cui, Yujun Shen, Kai Yang, Xin Lu, Yu Zheng, and Xinyi Le. 2022. A unified model for multi-class anomaly detection. *Advances in Neural Information Processing Systems* 35 (2022), 4571–4584.
- [40] Jiangning Zhang, Xuhai Chen, Yabiao Wang, Chengjie Wang, Yong Liu, Xiangtai Li, Ming-Hsuan Yang, and Dacheng Tao. 2023. Exploring plain vit reconstruction for multi-class unsupervised anomaly detection. *arXiv preprint arXiv:2312.07495* (2023).
- [41] Xuan Zhang, Shiyu Li, Xi Li, Ping Huang, Jiulong Shan, and Ting Chen. 2023. Destseg: Segmentation guided denoising student-teacher for anomaly detection. In *Proceedings of the IEEE/CVF Conference on Computer Vision and Pattern Recognition*. 3914–3923.
- [42] Yitian Zhang, Xu Ma, Yue Bai, Huan Wang, and Yun Fu. 2025. Accessing Vision Foundation Models via ImageNet-1K. In *The Thirteenth International Conference on Learning Representations*.
- [43] Jinghao Zhou, Chen Wei, Huiyu Wang, Wei Shen, Cihang Xie, Alan Yuille, and Tao Kong. 2021. ibot: Image bert pre-training with online tokenizer. *arXiv preprint arXiv:2111.07832* (2021).
- [44] Qihang Zhou, Guansong Pang, Yu Tian, Shibo He, and Jiming Chen. 2023. Anomalyclip: Object-agnostic prompt learning for zero-shot anomaly detection. *arXiv preprint arXiv:2310.18961* (2023).
- [45] Yang Zou, Jongheon Jeong, Latha Pemula, Dongqing Zhang, and Onkar Dabeer. 2022. Spot-the-difference self-supervised pre-training for anomaly detection and segmentation. In *European Conference on Computer Vision*. Springer, 392–408.

SUPPLEMENTARY

A Additional Ablation and Experiment

Pre-Trained Foundations. The representation quality of the frozen backbone Transformer is of great significance to FSAD. We conduct extensive experiments to probe the impact of different pre-training methods, including supervised learning and self-supervised learning. DeiT [34] is trained on ImageNet[9] in a supervised manner by distilling CNNs. Proteus [42] distills foundation models into smaller equivalents on ImageNet-1K. SynCLR [33] learns visual representations exclusively from synthetic images and synthetic captions, without relying on any real data. MAE [17], BEiTv2 [28], and DiGPT [30] are based on masked image modeling (MIM). MOCOV3 [5] is based on contrastive learning (CL), pulling the representations of the similar images and pushing those of different images. DINO [3] is based on positive-pair contrastive learning, which is also referred to as self-distillation. iBot [43] and DINOV2 [26] combine MIM and CL strategies, marking the SoTA of self-supervised foundation models. DINOV2-R [7] is a variation of DINOV2 that employs 4 extra register tokens. In addition, we evaluate the latest pre-training of large vision encoders, AIMv2, a family of open vision models pre-trained to autoregressively generate both image patches and text tokens.

It is worth noting that most models are pre-trained at a resolution of 224×224 , except for DINOV2 [26] and DINOV2-R [7], which include an additional high-resolution training phase at 392×392 . AIMv2 is pre-trained at 448×448 and 336×336 resolutions. Directly applying pre-trained weights to a different resolution in FSAD without fine-tuning can degrade performance, as shown in Table A3. Rather than significantly affecting pixel-level performance, the resolution mismatch has a more noticeable impact on image-level results. Proteus, DINOV2, and DINOV2-R, which are CL+MIM hybrid models, demonstrate better utilization of high-resolution inputs, confirming that strong backbone models can extract universal and discriminative features for FSAD. For example, the larger model AIMv2 also demonstrates performance that surpasses most other methods. In contrast, using MAE leads to the worst performance, which can be attributed to weak semantic representations induced by its pretraining strategy.

Input Size. To evaluate the impact of input resolution on VisionAD’s performance, we report its results under different resolutions, as shown in Table A2. Following PatchCore [31], we adopt center-crop preprocessing to reduce the influence of background regions. Experimental results demonstrate that VisionAD benefits from higher input resolutions for both anomaly detection and localization, while still achieving state-of-the-art performance even with smaller images. For fairness, all localization experiments are evaluated at a fixed resolution of 256×256 .

Scalability on MVTec and VisA under 1-/2-/4-shot setting. We demonstrate the performance of different ViT model sizes on MVTec and VisA under 1-/2-/4-shot setting in Table A1. The results show that larger models and more support images can lead to better performance. However, this also increases computational cost and slows down inference speed.

B Results Per-Category

For future research, we report the per-class results of MVTec-AD [1], VisA [45], and Real-IAD [35]. The performance of compared methods is drawn from KAG-prompt [32] and One-for-All [25]. The results of the 1-/2-/4-shot setting on MVTec-AD are presented in Table A4, Table A5 and Table A6, respectively. The results of the 1-/2-/4-shot setting on VisA are presented in Table A7, Table A8 and Table A9, respectively. The results of the 1-/2-/4-shot setting on Real-IAD are presented in Table A10.

C Qualitative Visualization

We visualize the output anomaly maps of VisionAD on MVTec-AD, VisA, and Real-IAD, as shown in Figure A2, Figure A3 and Figure A4. It is noted that all visualized samples are randomly chosen without artificial selection. It is shown that VisionAD has achieved anomaly localization results that closely match their ground truth. It not only effectively identifies larger anomalous regions but also detects subtle anomalies that are often overlooked. This demonstrates the exceptional anomaly localization capability of VisionAD. Such robustness and reliability under few-shot settings highlight the potential practical applicability of VisionAD in real-world scenarios.

D Failure Cases Study

To ensure a fair comparison with the INP on the Real-IAD dataset, we similarly selected only 1, 2, or 4 images per category as support samples. However, during the analysis of anomaly location (visualizations), we observed that VisionAD produced accurate results for images of the sample captured from similar views, whereas its performance noticeably degraded when the views varied significantly, as shown in Figure ???. This observation confirms our initial hypothesis that the notion of 1-/2-/4-shot should fundamentally refer to the number of samples rather than the number of images. Therefore, future research should consider collecting at least five distinct views per sample to construct the support set.

Table A1: Scaling of ViT model sizes on MVTec and VisA (%). Im/s (Throughput, image per second) is measured on NVIDIA RTX4090 with batch size=16. †:default.

Arch.	Params	MACs	Im/s	Setup	MVTec		VisA	
					AUROC	pAUROC	AUROC	pAUROC
ViT-Small	18.0M	14.2G	52.0	1-shot	96.3	95.6	91.3	96.8
				2-shot	96.9	96.1	92.4	97.1
				4-shot	97.3	96.4	94.1	97.5
ViT-Base†	71.3M	56.2G	26.6	1-shot	97.6	96.0	92.7	97.2
				2-shot	98.1	96.5	93.6	97.5
				4-shot	98.5	96.7	95.1	97.9
ViT-Large	239.9M	189.2G	10.1	1-shot	97.7	96.2	93.7	97.3
				2-shot	98.3	96.7	94.5	97.6
				4-shot	98.7	96.9	96.1	98.0

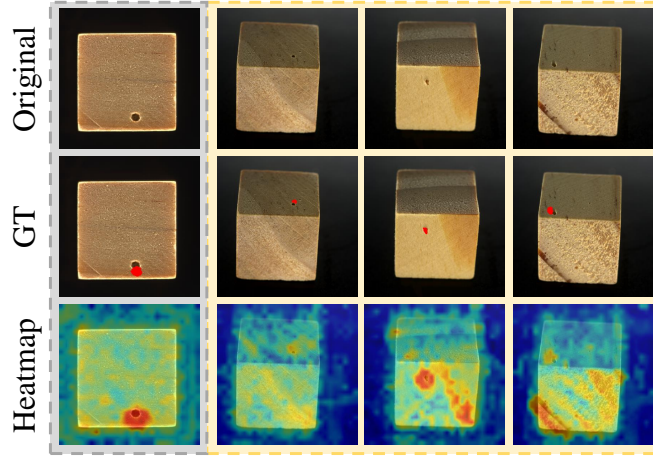


Figure A1: Failure case on Real-IAD: The first column shows samples that share the same view with the supports, while the last three columns show the anomaly maps under different views.

Table A2: Scaling input size on MVTec-AD (%). †: default.

Input Size	MACs	Setup	MVTec		VisA	
			AUROC	pAUROC	AUROC	pAUROC
R256 ² -C224 ²	18.6G	1-shot	95.5	95.4	88.6	96.1
		2-shot	96.5	96.1	89.8	96.4
		4-shot	97.0	96.3	91.2	97.0
R320 ² -C280 ²	28.9G	1-shot	97.2	95.7	90.9	96.9
		2-shot	97.7	96.3	91.8	97.1
		4-shot	98.1	96.5	93.4	97.6
R384 ² -C336 ²	41.4G	1-shot	97.5	95.9	91.5	97.2
		2-shot	98.1	96.4	92.5	97.4
		4-shot	98.5	96.6	94.2	97.8
R448 ² -C392 ² †	56.2G	1-shot	97.6	96.0	92.7	97.2
		2-shot	98.1	96.5	93.6	97.5
		4-shot	98.5	96.7	95.1	97.9
R512 ² -C448 ²	73.4G	1-shot	97.6	96.1	93.3	97.3
		2-shot	98.3	96.5	94.1	97.6
		4-shot	98.7	96.7	95.9	97.9

Table A3: Comparison between pre-trained ViT foundations under 1-shot setting, conducted on MVTec-AD and VisA (%). All models except AIMv2 are ViT-Base. The patch size for AIMv2, DINov2, and DINov2-R is 14^2 , while for the others it is 16^2 . $R448^2\text{-}C392^2$ represents first resizing images to 448×448 , then center cropping to 392×392 .

Pre-Train Backbone	Type	Image Size	MVTec				VisA			
			AUROC	AUPR	pAUROC	PRO	AUROC	AUPR	pAUROC	PRO
DeiT [34]	Supervised	$R512^2\text{-}C448^2$	86.21	93.33	92.31	81.17	86.34	87.93	95.46	83.04
Proteus [42]	Supervised	$R448^2\text{-}C392^2$	95.89	98.21	96.11	90.41	89.23	90.04	96.37	82.46
SynCLR [33]	Supervised	$R448^2\text{-}C384^2$	82.18	96.69	95.57	88.04	87.92	89.40	96.58	85.78
MAE [17]	MIM	$R512^2\text{-}C448^2$	72.75	86.95	86.79	70.11	70.31	73.45	85.64	67.13
D-iGPT [30]	MIM	$R512^2\text{-}C448^2$	86.92	93.60	94.47	84.10	87.85	88.86	95.75	84.72
MOCOV3 [5]	CL	$R512^2\text{-}C448^2$	88.10	94.03	94.71	85.48	85.45	86.94	96.07	84.25
DINO [3]	CL	$R512^2\text{-}C448^2$	88.83	94.87	95.13	86.53	85.32	87.06	96.66	86.23
iBOT [43]	CL+MIM	$R512^2\text{-}C448^2$	88.66	94.76	95.46	86.83	85.18	87.16	96.70	85.79
DINov2 [26]	CL+MIM	$R448^2\text{-}C392^2$	97.05	98.88	95.89	91.74	93.44	93.56	97.37	90.78
DINov2-R [7]	CL+MIM	$R448^2\text{-}C392^2$	97.60	99.11	96.01	91.86	92.66	92.74	97.22	90.93
DeiT[34]	Supervised	$R256^2\text{-}C224^2$	88.62	95.33	92.90	80.39	81.30	84.28	93.24	70.91
Proteus [42]	Supervised	$R256^2\text{-}C224^2$	94.95	97.95	95.72	88.88	89.23	90.04	96.37	82.46
SynCLR [33]	Supervised	$R256^2\text{-}C224^2$	92.44	96.87	95.51	87.82	84.70	86.67	94.92	75.43
MAE [17]	MIM	$R256^2\text{-}C224^2$	74.39	87.64	89.45	70.36	64.77	69.53	85.43	55.20
BEiT2 [28]	MIM	$R256^2\text{-}C224^2$	93.26	97.30	94.50	86.17	86.04	86.67	93.20	70.96
D-iGPT [30]	MIM	$R256^2\text{-}C224^2$	89.95	95.59	94.58	84.95	86.82	88.93	94.67	78.19
MOCOV3 [5]	CL	$R256^2\text{-}C224^2$	89.29	95.81	94.14	83.15	85.45	86.94	96.07	84.25
DINO [3]	CL	$R256^2\text{-}C224^2$	89.92	96.07	94.57	84.64	81.15	83.95	94.95	74.97
iBOT [43]	CL+MIM	$R256^2\text{-}C224^2$	89.73	96.02	94.97	84.98	81.48	84.22	94.96	75.09
DINov2 [26]	CL+MIM	$R256^2\text{-}C224^2$	95.23	98.05	95.42	88.74	89.23	90.28	96.03	81.66
DINov2-R [7]	CL+MIM	$R256^2\text{-}C224^2$	95.53	98.23	95.41	88.96	88.55	89.80	96.12	82.66
AIMv2-large-patch14-336 [10]	Supervised	$R384^2\text{-}C336^2$	93.99	97.32	94.53	88.99	90.32	91.29	96.50	88.31
AIMv2-huge-patch14-336 [10]	Supervised	$R384^2\text{-}C336^2$	93.72	97.00	94.17	88.49	90.59	91.93	96.72	88.68
AIMv2-1B-patch14-336 [10]	Supervised	$R384^2\text{-}C336^2$	94.33	97.36	93.92	88.67	91.71	92.89	96.87	89.50
AIMv2-3B-patch14-336 [10]	Supervised	$R384^2\text{-}C336^2$	95.32	97.98	93.90	88.09	92.17	93.40	96.70	89.04
AIMv2-large-patch14-448 [10]	Supervised	$R512^2\text{-}C448^2$	93.89	97.21	94.04	88.97	92.62	93.19	96.56	90.21
AIMv2-huge-patch14-448 [10]	Supervised	$R512^2\text{-}C448^2$	93.52	96.86	93.51	88.08	92.68	93.84	96.64	90.11
AIMv2-1B-patch14-448 [10]	Supervised	$R512^2\text{-}C448^2$	94.25	97.24	93.51	88.58	93.38	94.27	96.76	90.41
AIMv2-3B-patch14-448 [10]	Supervised	$R512^2\text{-}C448^2$	95.04	97.67	93.06	87.42	93.80	94.39	96.60	90.46

Table A4: Subset-wise performance comparison results of the 1-shot setting for AUROC/AP/pAUROC/PRO on MVTecAD.

Method →	PatchCore [31] CVPR'22	WinCLIP [19] CVPR'23	APRIL-GAN [4] arXiv'23	AnomalyGPT [11] AAAI'24	PromptAD [20] CVPR'24	KAG-prompt [32] AAAI'25	One-for-All [25] ICLR'25	VisionAD Ours								
Category ↓	Bottle	Cable	Capsule	Hazelnut	Screw	Metal nut	Pill	Toothbrush	Transistor	Zipper	Carpet	Grid	Leather	Tile	Wood	Mean
Objects	99.4/99.8/97.9/93.5 98.2/99.4/97.5/91.2 99.9/100.0/98.7/96.5 98.1/98.7/97.6/94.4 99.8/99.8/99.6/93.6 98.7/99.6/97.5/93.9 99.7/99.9/98.4/94.9 97.3±0.3/88.3±0.1/96.6±0.0/93.3±0.1	88.8/93.8/95.5/84.7 88.9/93.2/93.8/72.5 92.8/97.8/96.4/92.7 88.8/93.1/93.1/83.5 94.2/95.5/98.4/87.3 90.7/94.5/91.6/80.8 92.8/96.1/94.9/86.7 93.1±0.7/96.5±0.3/93.4±0.4/85.4±1.1	67.8/89.4/95.6/83.9 72.3/91.6/94.6/85.6 98.5/99.3/97.6/92.1 90.1/97.8/92.3/85.5 84.6/97.8/99.5/80.1 90.9/98.0/97.4/93.6 80.5/95.4/97.2/91.3 95.4±1.8/99.9±0.4/97.5±0.2/96.2±0.2	88.3/92.9/95.8/88.3 97.5/98.6/98.5/93.7 92.0/98.3/97.1/95.6 100/100./98.6/95.6 99.8/99.7/97.3/92.9 100./100./98.5/94.2 98.0/99.2/98.4/93.8 99.7±0.4/99.8±0.2/99.3±0.1/96.3±1.0	44.4/71.4/93.1/89.5 86.4/94.2/96.4/93.5 88.5/97.4/80.4/64.8 74.7/88.2/95.9/94.6 65.0/78.5/98.4/90.8 73.1/89.0/96.8/96.2 96.6/99.4/96.4/96.4 84.4±7.1/94.2±2.9/98.5±0.5/94.2±1.5	73.4/91.0/89.3/66.7 98.7/99.7/90.0/84.7 84.6/97.0/94.8/96.6 98.3/94.8/90.6/87.0 99.1/99.6/97.3/83.1 99.9/100.0/93.7/91.5 99.4/99.9/94.4/91.8 97.2±1.0/99.4±2.0/90.4±0.6/86.5±0.8	81.9/96.5/93.1/89.5 91.2/98.3/96.4/93.5 83.4/76.1/80.4/64.8 94.6/98.7/95.9/94.6 92.6/98.5/98.4/90.8 94.8/99.1/96.8/96.2 96.6/99.4/96.6/94.8 98.0±0.2/99.7±0.0/91.6±0.4/95.4±0.3	83.3/93.5/97.3/79.0 92.2/96.7/97.8/85.3 94.3/97.8/98.4/93.4 98.4/99.1/98.2/90.8 98.9/98.5/94.0/90.1 99.2/99.7/98.6/91.7 91.9/97.3/97.4/98.2 98.8±0.8/99.6±0.3/99.0±0.3/95.6±0.3	78.1/77.7/84.9/70.9 83.4/79.0/80.5/65.0 94.3/98.3/96.1/87.2 97.2/68.5/87.6/71.2 94.0/91.2/99.1/67.5 93.9/92.1/84.6/65.0 94.1/89.8/86.8/67.4 98.8±0.7/98.5±0.5/86.7±3.2/73.5±2.6	92.3/97.2/97.4/91.2 88.8/96.8/93.9/86.0 98.5/99.5/96.1/95.9 97.2/99.0/93.8/84.8 93.9/99.0/96.6/81.0 98.9/99.7/97.3/91.7 89.4/95.6/96.0/88.3 99.4±0.6/99.8±0.2/97.4±0.2/93.1±0.8	95.3/98.7/98.4/93.3 99.8/99.9/99.4/97.4 99.9/100.0/99.5/99.0 99.8/99.9/99.1/96.8 100.0/100.0/95.9/98.3 100.0/100.0/99.4/97.3 100.0/100.0/99.5/98.1 99.9±0.2/100.±0.0/99.4±0.1/97.7±0.4	63.6/81.1/58.8/21.7 99.5/99.9/96.8/90.5 74.7/84.8/90.8/81.5 98.4/98.6/95.9/90.9 99.8/98.8/95.1/94.3 99.1/99.7/97.0/92.1 97.0/99.0/96.6/88.4 99.3±0.4/99.8±0.1/99.4±0.1/97.6±0.4	97.3/99.1/98.5/95.2 99.9/100.0/99.3/98.6 99.0/99.6/96.9/90.2 100.0/100.0/99.3/97.9 100.0/100.0/99.3/98.7 100.0/100.0/99.5/98.1 100.0/100.0/99.4/98.7 100.±0.0/100.±0.0/99.1±0.1/97.1±0.6	93.2/96.0/96.3/89.8 98.3/99.1/98.7/94.2 92.1/98.4/97.1/96.0 100.0/100.0/98.7/95.7 99.4/99.8/97.6/93.4 100.0/100.0/98.5/94.2 98.5/99.4/98.7/94.6 99.9±0.1/100.±0.0/99.3±0.1/96.7±0.4	97.8/99.3/92.7/87.1 99.9/100.0/94.6/91.0 98.9/99.6/95.4/92.3 98.1/98.5/96.4/93.2 97.9/99.6/89.4/92.4 98.8/99.6/96.4/93.4 99.4/99.8/97.0/94.2 99.1±0.4/99.7±0.1/96.8±0.4/94.2±0.5	83.4/92.2/92.0/79.3 93.1/96.5/95.2/87.1 92.0/95.8/95.1/90.6 94.1/95.9/95.3/89.5 94.6/97.1/95.9/87.9 95.8/98.1/96.2/90.8 94.2/97.2/96.4/89.8 97.4±0.4/99.0±0.2/96.2±0.2/92.5±0.3
	99.2/98.8/98.1/93.9 99.3/99.8/97.7/91.8 99.9/100.0/98.7/96.7 99.4/99.8/97.7/94.7 100.0/99.9/99.5/93.9 99.6/99.9/97.7/94.4 99.8/100.0/98.6/95.2 98.7±0.0/99.6±0.2/97.2±0.1/94.3±0.2	91.0/95.1/96.4/88.5 88.4/92.9/94.3/74.7 94.0/98.2/96.9/93.6 90.4/93.9/93.2/84.2 99.9/96.9/97.6/87.8 91.2/95.0/92.4/81.7 92.1/95.8/95.3/89.5 94.7±0.7/97.3±0.3/94.0±0.5/96.9±0.7	72.8/91.0/96.5/86.6 77.3/93.3/96.4/90.6 98.7/99.4/97.7/92.5 89.8/97.7/92.3/85.7 100.0/97.0/99.3/97.2 91.1/98.0/97.7/94.3 91.8/98.3/97.5/92.6 95.4±1.8/99.0±0.4/97.7±0.2/96.7±0.2	93.2/96.0/96.3/89.8 98.3/99.1/98.7/94.2 92.1/98.4/97.1/96.0 100.0/100.0/98.7/95.7 99.4/99.8/97.6/93.4 100.0/100.0/98.5/94.2 98.5/99.4/98.7/94.6 99.9±0.1/100.±0.0/99.3±0.1/96.7±0.4	49.0/72.9/90.0/69.0 86.0/94.1/95.2/84.1 90.5/97.8/92.1/90.5 83.5/94.3/95.6/86.0 98.6/86.7/95.1/74.7 82.4/94.0/97.3/88.9 81.5/92.6/95.6/85.8 88.9±4.8/96.2±1.8/98.8±0.4/95.6±1.5	77.7/92.3/94.6/79.6 99.4/99.9/91.4/86.7 84.1/96.9/95.0/96.7 100.0/100.0/91.6/87.8 91.3/100.0/97.4/87.7 99.9/100.0/94.5/92.3 99.7/99.9/95.4/92.3 99.2±0.3/99.8±0.1/92.9±0.8/89.7±0.8	82.9/96.6/94.2/91.6 92.3/93.8/96.7/90.45 83.8/77.5/82.5/66.5 95.9/99.3/96.9/95.6 100.0/97.8/98.5/90.5 94.6/99.0/96.9/96.3 96.0/99.3/97.0/94.1 98.3±0.2/99.7±0.0/92.1±0.3/95.6±0.1	85.9/94.1/97.5/81.0 97.5/99.0/98.1/84.7 94.8/98.0/98.5/93.8 99.2/99.7/98.3/90.9 71.0/99.3/95.5/91.6 98.9/99.6/98.7/91.9 92.5/97.5/97.5/94.2 98.9±0.7/99.6±0.3/99.1±0.3/96.1±0.4	90.0/89.3/89.6/78.8 85.3/80.7/88.3/68.6 94.7/98.4/96.4/88.7 80.4/69.3/88.4/73.5 97.5/92.2/99.0/68.1 95.0/93.6/86.1/67.1 90.4/88.3/88.4/68.6 99.4±0.3/99.2±0.5/88.4±1.4/75.4±1.5	94.0/97.8/98.0/92.8 94.0/98.3/94.1/86.4 98.7/99.6/96.1/96.0 96.2/99.0/93.9/84.9 95.8/99.3/95.5/86.4 98.5/99.6/97.3/91.5 95.5/98.7/96.7/89.6 99.4±0.9/99.8±0.3/97.6±0.1/93.6±0.4	96.6/99.0/98.5/93.7 99.8/99.9/99.3/97.3 100.0/100.0/99.5/99.0 100.0/100.0/99.4/97.3 100.0/100.0/99.5/97.5 100.0/100.0/99.5/98.0 99.9±0.1/100.±0.0/99.4±0.0/97.7±0.3	67.7/84.1/62.6/23.7 99.4/99.8/97.7/92.8 74.9/95.8/91.2/82.9 94.4/99.8/96.5/91.3 98.7/99.9/95.5/95.0 99.2/99.7/97.1/92.0 97.0/99.0/96.3/87.7 99.5±0.2/99.8±0.1/99.4±0.0/97.7±0.1	97.9/99.3/99.0/95.9 99.9/100.0/99.3/98.3 99.0/99.6/96.9/90.9 100.0/100.0/99.3/97.9 91.8/100.0/93.2/98.7 100.0/100.0/99.5/98.0 100.0/100.0/99.3/98.5 100.±0.0/100.±0.0/99.1±0.1/97.0±0.4	98.5/94.4/94.8/82.5 95.9/99.0/96.5/89.6 82.0/92.4/98.3/93.1 99.5/99.8/96.2/90.7 93.6/100.0/94.1/90.9 99.9/99.9/97.8/89.3 99.5/99.8/97.1/90.7 99.9±0.1/100.±0.0/97.6±0.1/90.5±0.4	98.3/99.5/93.2/86.8 99.9/100.0/95.3/91.8 99.0/99.6/95.8/92.3 99.1/99.7/96.4/93.4 97.4/99.7/89.1/91.6 98.4/99.5/96.3/92.8 99.2/99.8/97.3/94.6 99.2±0.3/99.7±0.1/97.6±0.1/94.7±0.2	86.3/93.8/93.3/82.3 94.3/97.4/96.0/88.4 92.4/96.0/95.5/91.3 95.5/96.8/95.6/90.0 95.7/97.9/96.2/88.5 96.6/98.5/96.5/91.1 95.6/97.9/96.7/90.3 98.1±0.3/99.3±0.1/96.6±0.1/93.2±0.2
	99.2/98.8/98.2/94.0 99.3/99.8/97.8/91.6 99.9/100.0/98.7/96.6 99.4/99.8/98.2/95.2 100.0/100.0/99.5/94.5 99.5/99.9/98.0/94.6 99.1/99.7/98.6/95.5 99.3±0.8/99.8±0.2/97.5±0.1/94.6±0.2	91.0/97.1/95.7/91.7 90.9/94.4/94.9/77.0 94.2/98.3/97.2/94.3 91.4/95.4/94.3/85.6 98.8/97.4/98.2/88.9 91.5/95.3/92.5/82.0 95.4/97.5/96.4/91.2 94.8±1.5/97.4±0.6/94.2±0.4/87.5±0.5	72.8/94.9/96.8/87.8 83.2/95.1/96.2/90.1 98.8/99.4/97.9/92.6 91.1/98.5/93.4/87.1 100.0/98.6/99.3/88.7 92.9/98.4/97.9/94.9 94.5/98.9/97.2/88.9 96.9±0.3/99.3±0.0/98.0±0.1/97.1±0.1	93.2/97.0/97.6/92.0 98.4/99.1/98.8/94.2 93.5/98.7/97.5/96.6 100.0/100.0/98.8/96.3 99.8/99.9/97.9/95.2 100.0/100.0/98.7/94.7 98.5/99.4/98.8/95.8 100.±0.0/100.±0.0/99.4±0.0/97.1±0.3	49.0/71.8/91.3/72.4 87.9/94.9/96.0/86.3 91.0/97.9/93.1/91.7 84.8/94.5/96.8/87.6 100.0/93.8/94.9/86.7 84.7/94.7/97.5/89.8 82.1/92.0/96.9/87.5 92.3±1.0/97.4±0.3/99.1±0.1/96.5±0.4	77.7/92.0/95.9/83.8 99.5/99.9/92.9/89.4 84.1/96.9/95.5/96.7 100.0/100.0/93.4/90.1 91.5/99.9/97.7/87.6 100.0/100.0/94.6/92.4 99.9/100.0/94.6/93.4 99.4±0.4/99.9±0.1/93.6±0.7/90.4±0.7	82.9/96.9/94.8/92.5 92.8/98.6/97.1/94.6 84.1/78.1/83.7/67.7 95.8/99.3/97.2/96.1 99.8/98.5/98.5/92.0 95.1/99.1/97.0/96.5 96.6/99.4/96.9/95.6 98.4±0.3/99.7±0.1/92.6±0.3/95.8±0.1	85.9/94.8/98.4/85.5 96.7/98.7/98.4/86.0 93.2/97.3/98.8/94.8 98.1/98.3/98.3/90.9 83.6/99.7/96.2/91.3 99.2/99.7/98.7/91.9 92.5/97.5/97.9/84.4 99.8±0.2/99.9±0.1/99.3±0.1/96.7±0.3	90.0/84.5/90.7/79.5 85.7/80.7/88.5/69.0 95.4/98.6/96.8/92.2 88.3/83.1/90.2/74.9 98.1/92.2/99.0/73.0 96.9/96.5/86.6/67.4 91.2/89.2/89.6/71.2 99.6±0.2/99.4±0.4/89.7±0.5/78.3±0.6	94.0/99.5/98.1/93.4 94.5/98.5/94.2/86.9 98.7/99.6/96.2/96.1 97.5/97.3/94.1/85.3 95.0/98.5/96.6/87.5 99.1/99.8/97.7/92.7 96.0/98.8/96.7/90.8 99.9±0.1/100.±0.0/97.8±0.1/94.1±0.3	96.6/98.8/96.9/93.9 100.0/100.0/99.3/97.0 100.0/100.0/99.4/97.3 100.0/100.0/96.2/98.2 100.0/100.0/99.5/97.4 100.0/100.0/99.5/97.7 99.9±0.1/100.±0.0/99.4±0.0/97.6±0.2	67.7/86.4/69.4/30.4 99.6/99.9/98.0/93.6 76.7/86.5/91.8/84.0 99.4/99.7/96.9/93.5 98.6/99.7/95.2/93.8 99.2/99.7/96.7/93.3 96.0/98.6/98.1/91.3 99.5±0.3/99.8±0.1/99.4±0.0/97.6±0.1	97.9/99.6/99.1/96.4 100.0/100.0/99.3/98.0 99.2/99.7/97.6/92.0 100.0/100.0/99.3/97.7 95.4/100.0/93.9/98.4 100.0/100.0/99.5/97.9 100.0/100.0/99.5/98.6 100.±0.0/100.±0.0/99.0±0.1/96.7±0.5	98.5/99.6/94.8/83.0 99.9/100.0/96.0/89.9 83.7/93.2/98.5/93.7 99.2/99.7/96.3/90.4 92.9/100.0/94.1/90.9 99.9/99.9/97.3/91.2 100.±0.0/100.±0.0/97.6±0.0/90.4±0.5	98.3/99.5/93.5/87.7 99.8/99.9/95.4/91.7 99.1/99.6/96.0/92.4 99.5/99.0/96.4/92.6 95.6/99.5/90.6/91.4 98.6/99.5/96.2/92.7 99.6/99.9/97.4/94.7 99.1±0.4/99.7±0.2/97.3±0.3/94.9±0.4	

Table A5: Subset-wise performance comparison results of the 2-shot setting for AUROC/AP/pAUROC/PRO on MVTecAD.

Method →	PatchCore [31] CVPR'22	WinCLIP [19] CVPR'23	APRIL-GAN [4] arXiv'23	AnomalyGPT [11] AAAI'24	PromptAD [20] CVPR'24	KAG-prompt [32] AAAI'25	One-for-All [25] ICLR'25	VisionAD Ours								
Category ↓	Bottle	Cable	Capsule	Hazelnut	Screw	Metal nut	Pill	Toothbrush	Transistor	Zipper	Carpet	Grid	Leather	Tile	Wood	Mean
Objects	99.2/98.8/98.2/94.0 99.3/99.8/97.8/91.6 99.9/100.0/98.7/96.6 99.4/99.8/98.2/95.2 100.0/100.0/99.5/94.5 99.5/99.9/98.0/94.6 99.1/99.7/98.6/95.5 99.3±0.8/99.8±0.2/97.5±0.1/94.6±0.2	91.0/97.1/95.7/91.7 90.9/94.4/94.9/77.0 94.2/98.3/97.2/94.3 91.4/95.4/94.3/85.6 98.8/97.4/98.2/88.9 91.5/95.3/92.5/82.0 95.4/97.5/96.4/91.2 94.8±1.5/97.4±0.6/94.2±0.4/87.5±0.5	72.8/94.9/96.8/87.8 83.2/95.1/96.2/90.1 98.8/99.4/97.9/92.6 91.1/98.5/93.4/87.1 100.0/98.6/99.3/88.7 92.9/98.4/97.9/94.9 94.5/98.9/97.2/88.9 96.9±0.3/99.3±0.0/98.0±0.1/97.1±0.1	93.2/97.0/97.6/92.0 98.4/99.1/98.8/94.2 93.5/98.7/97.5/96.6 100.0/100.0/98.8/96.3 99.8/99.9/97.9/95.2 100.0/100.0/98.7/94.7 98.5/99.4/98.8/95.8 100.±0.0/100.±0.0/99.4±0.0/97.1±0.3	49.0/71.8/91.3/72.4 87.9/94.9/96.0/86.3 91.0/97.9/93.1/91.7 84.8/94.5/96.8/87.6 100.0/93.8/94.9/86.7 84.7/94.7/97.5/89.8 82.1/92.0/96.9/87.5 92.3±1.0/97.4±0.3/99.1±0.1/96.5±0.4	77.7/92.0/95.9/83.8 99.5/99.9/92.9/89.4 84.1/96.9/95.5/96.7 100.0/100.0/93.4/90.1 91.5/99.9/97.7/87.6 100.0/100.0/94.6/92.4 99.9/100.0/										

Table A7: Subset-wise performance comparison results of the 1-shot setting for AUROC/AP/pAUROC/PRO on VisA.

Method →	PatchCore [31] CVPR'22	WinCLIP [19] CVPR'23	APRIL-GAN [4] arXiv'23	AnomalyGPT [11] AAAI'24	PromptAD [20] CVPR'24	KAG-prompt [32] AAAI'25	One-for-All [25] ICLR'25	VisionAD Ours
Category ↓								
pcb1	78.9/72.1/96.1/79.0	75.6/76.5/96.6/82.5	89.0/90.2/95.3/90.4	82.6/76.0/97.9/83.1	88.7/88.0/96.6/89.2	84.4/81.0/97.4/85.8	83.5/77.4/98.5/84.3	93.7±0.9/92.7±1.2/98.8±0.1/90.1±0.6
pcb2	81.5/84.4/95.4/80.9	62.2/64.9/93.0/73.6	85.4/87.1/92.5/79.2	75.6/76.9/92.5/64.9	71.6/75.4/93.5/79.3	83.3/86.8/94.0/67.7	72.6/70.2/94.6/77.3	92.9±2.1/93.4±2.0/95.8±0.5/83.1±2.6
pcb3	82.7/84.6/96.2/78.1	74.1/73.5/94.3/79.5	87.8/89.4/93.2/81.3	75.0/79.9/94.6/69.9	97.1/75.2/95.9/84.0	81.4/83.2/95.6/75.7	71.8/73.2/93.0/76.8	94.4±2.4/94.8±2.1/97.2±0.6/88.3±1.9
pcb4	93.9/92.8/95.6/77.9	85.2/78.5/94.0/76.6	97.5/97.0/95.8/89.3	88.8/81.9/94.9/75.9	91.4/90.5/95.5/78.8	97.9/97.5/96.9/83.8	82.9/80.9/95.2/83.7	99.4±0.2/99.4±0.2/95.0±1.1/83.2±3.7
macaroni1	68.0/67.8/95.2/83.4	82.9/84.9/96.4/84.6	89.7/92.0/99.3/95.3	89.9/92.8/97.6/87.5	88.6/86.3/97.8/87.5	96.6/97.0/98.6/92.0	85.1/89.3/97.5/89.3	93.8±3.3/94.4±2.8/99.4±0.2/94.7±0.7
macaroni2	55.6/54.9/89.1/66.0	70.2/68.4/96.8/89.3	79.2/83.4/98.4/85.6	84.7/87.1/95.3/82.6	69.1/72.5/96.6/80.6	84.1/88.1/97.3/87.7	75.5/79.3/96.6/86.6	79.8±3.9/74.9±4.8/98.8±0.5/94.4±1.5
capsules	60.0/72.3/93.2/66.6	85.0/89.9/96.4/73.6	92.7/95.8/98.0/88.4	85.8/91.4/97.6/82.4	84.5/90.1/95.4/70.0	89.1/94.1/97.5/78.9	88.9/94.7/97.1/83.6	96.4±0.5/97.9±0.3/97.7±0.4/94.6±1.0
candle	85.1/86.7/97.2/92.6	93.4/93.6/97.4/94.0	90.9/91.6/98.7/96.4	85.8/86.4/98.2/91.7	90.3/93.7/95.8/91.8	96.3/96.8/98.6/92.5	91.9/94.1/98.5/95.0	95.2±1.3/96.1±1.0/99.0±0.1/94.4±0.6
cashew	89.5/94.6/98.1/90.8	94.0/97.2/98.5/91.1	93.4/97.1/90.8/94.2	91.5/96.3/96.5/90.5	95.6/97.6/99.1/92.3	94.4/97.6/98.6/92.7	85.6/95.7/97.6/92.9	96.3±1.0/98.1±0.5/98.1±0.3/96.1±0.8
chewinggum	97.3/98.9/96.7/82.4	97.6/99.0/98.6/91.0	97.3/99.0/99.7/92.1	98.0/99.1/99.1/87.3	96.4/99.1/99.1/89.8	98.7/99.4/99.2/88.2	97.7/99.1/99.6/92.5	99.5±0.1/99.8±0.0/99.4±0.0/94.2±0.2
pipe_fryum	90.7/95.4/98.8/93.6	97.2/98.6/98.3/96.1	98.3/99.2/97.3/96.1	99.3/99.7/98.0/95.9	96.9/98.3/99.1/95.2	99.5/99.8/98.4/95.6	99.8/99.9/98.3/97.2	98.3±1.0/99.2±0.5/98.6±0.1/96.2±0.4
fryum	75.0/87.6/93.3/78.7	88.5/94.7/96.4/89.1	93.4/97.3/93.6/91.5	92.2/96.4/92.7/83.1	90.3/93.8/95.4/83.5	93.7/97.5/93.8/81.6	89.9/96.3/96.2/87.7	97.6±0.3/98.9±0.1/93.1±0.7/89.3±1.1
Mean	79.9/82.8/95.4/80.5	83.8/85.1/96.4/85.1	91.2/93.3/96.0/90.0	87.4/88.7/96.2/82.9	86.9/88.4/96.7/85.1	91.6/93.2/97.0/85.2	85.4/87.5/96.9/87.3	94.8±1.0/95.0±0.9/97.6±0.3/91.6±0.8

Table A8: Subset-wise performance comparison results of the 2-shot setting for AUROC/AP/pAUROC/PRO on VisA.

Method →	PatchCore [31] CVPR'22	WinCLIP [19] CVPR'23	APRIL-GAN [4] arXiv'23	AnomalyGPT [11] AAAI'24	PromptAD [20] CVPR'24	KAG-prompt [32] AAAI'25	One-for-All [25] ICLR'25	VisionAD Ours
Category ↓								
pcb1	71.5/72.6/97.6/86.1	76.7/78.3/97.0/83.8	90.9/91.6/95.8/90.6	83.6/78.7/96.5/82.9	90.9/80.9/96.9/90.2	88.8/86.7/98.0/87.0	86.5/78.5/98.5/85.1	93.3±0.6/92.1±0.9/98.8±0.1/90.1±0.5
pcb2	84.3/86.6/96.0/82.9	62.6/65.8/93.9/76.2	89.2/91.3/92.8/79.7	78.3/75.8/93.0/64.8	73.0/73.0/94.8/79.3	82.0/85.2/95.2/73.9	75.2/73.6/96.8/77.8	93.3±0.4/93.4±0.9/96.0±0.1/83.6±0.8
pcb3	84.8/86.1/97.1/82.2	78.8/80.9/95.1/82.3	90.9/92.2/93.5/81.5	79.2/80.4/95.9/72.4	76.2/82.8/96.1/84.7	89.0/90.0/95.6/75.5	70.7/74.3/93.7/78.7	93.5±3.5/94.2±2.6/97.4±0.3/89.2±1.5
pcb4	94.3/93.2/96.2/79.5	82.3/72.5/95.6/81.7	97.9/97.8/95.9/89.5	88.4/81.8/95.3/77.8	97.5/94.5/95.6/78.3	97.2/96.8/97.3/85.5	84.4/81.7/96.6/84.3	99.2±0.3/99.1±0.3/95.2±0.2/83.2±1.3
macaroni1	75.6/74.9/96.0/86.2	83.3/84.7/96.5/85.2	90.0/92.2/99.3/95.2	91.4/92.8/96.8/87.4	84.2/91.1/98.3/90.6	95.9/97.0/98.9/92.5	84.7/90.7/97.6/90.1	96.4±0.6/96.7±0.7/99.5±0.1/95.2±0.4
macaroni2	57.3/57.2/90.2/67.2	71.8/70.4/96.8/88.6	81.0/85.1/98.4/85.4	85.8/88.6/96.3/83.1	82.6/84.7/97.2/82.7	86.9/89.8/97.4/87.1	76.1/73.6/96.9/86.3	80.0±3.1/76.8±6.0/98.9±0.3/94.6±1.1
capsules	57.8/73.6/94.0/67.9	84.9/88.9/96.8/75.9	93.4/96.3/98.0/89.1	88.8/94.3/98.3/85.7	84.9/88.3/96.1/70.8	89.9/95.0/98.4/85.9	90.3/94.9/97.3/83.9	97.0±1.4/98.3±0.7/97.7±0.3/94.7±0.3
candle	85.3/86.8/97.7/93.4	94.8/95.1/97.7/94.2	91.3/91.9/98.6/96.5	83.1/83.2/98.3/91.8	91.0/93.6/95.9/91.6	94.5/95.3/98.8/92.7	95.5/95.3/98.5/95.3	96.2±0.7/96.9±0.6/99.1±0.4/94.7±0.5
cashew	93.6/96.9/98.2/91.4	94.3/97.3/98.5/90.4	93.4/97.2/90.8/94.1	93.2/96.1/95.7/89.8	94.7/97.4/99.2/92.7	94.3/97.3/98.2/92.5	86.7/95.2/97.1/93.0	96.9±0.9/98.4±0.4/98.1±0.1/96.6±0.5
chewinggum	97.8/99.1/96.6/78.0	97.3/98.9/96.8/90.9	97.1/98.9/99.7/92.1	98.4/99.1/98.7/85.4	96.6/98.4/99.2/88.0	98.8/99.5/99.2/88.0	97.8/99.2/99.5/93.4	99.5±0.1/99.8±0.0/99.4±0.0/93.9±0.4
pipe_fryum	93.5/96.8/99.1/94.5	98.0/99.0/98.5/96.2	98.4/99.3/97.3/96.1	99.4/99.7/98.2/95.9	98.9/99.1/99.4/94.8	99.7/99.9/98.4/95.8	99.9/100.0/98.5/97.1	98.5±0.7/99.2±0.3/98.6±0.1/96.4±0.6
fryum	83.4/92.1/94.0/81.4	90.5/95.8/97.0/89.3	93.1/97.2/93.6/91.6	94.1/97.5/93.6/83.2	89.2/96.0/96.4/86.2	95.1/97.9/93.8/84.2	92.7/96.8/96.1/88.1	96.3±2.3/98.3±1.0/93.3±0.3/89.3±0.9
Mean	81.6/84.8/96.1/82.6	84.6/85.8/96.8/86.2	92.2/94.2/96.2/90.1	88.6/89.0/96.4/83.4	88.3/90.0/97.1/85.8	92.7/94.2/97.4/86.7	86.7/88.6/97.2/87.9	95.0±0.3/95.2±0.6/97.7±0.0/91.8±0.3

Table A9: Subset-wise performance comparison results of the 4-shot setting for AUROC/AP/pAUROC/PRO on VisA.

Method →	PatchCore [31] CVPR'22	WinCLIP [19] CVPR'23	APRIL-GAN [4] arXiv'23	AnomalyGPT [11] AAAI'24	PromptAD [20] CVPR'24	KAG-prompt [32] AAAI'25	One-for-All [25] ICLR'25	VisionAD Ours
Category ↓								
pcb1	84.7/81.0/98.1/88.1	88.3/87.7/98.1/87.9	91.2/91.8/96.0/90.6	83.1/77.1/96.8/83.1	90.9/90.1/98.2/90.2	89.7/87.6/97.9/87.2	85.2/78.6/98.7/85.6	93.8±0.7/92.9±1.4/98.9±0.1/90.9±0.3
pcb2	84.3/86.2/96.6/83.7	67.5/71.3/94.6/78.0	89.2/91.3/93.0/80.2	85.5/86.7/93.2/71.3	78.6/75.3/95.3/76.3	87.8/90.7/96.1/77.7	75.5/73.9/96.6/77.4	94.4±0.9/94.7±1.0/96.3±0.1/85.0±0.9
pcb3	87.0/88.3/97.4/84.4	83.3/84.8/95.8/84.2	91.6/92.7/93.7/81.5	86.9/88.3/96.1/73.1	80.3/83.5/96.8/85.0	85.8/86.9/96.4/78.6	74.7/74.6/94.0/78.1	96.7±0.6/96.9±0.5/97.9±0.1/90.3±0.7
pcb4	95.6/94.9/97.0/83.5	87.6/85.6/96.1/84.2	98.2/98.0/96.0/89.7	91.2/87.1/95.6/79.1	97.8/97.5/96.2/83.4	97.4/97.0/96.7/87.0	88.7/84.5/97.2/87.3	99.5±0.2/99.4±0.2/96.1±0.1/86.2±1.0
macaroni1	82.9/82.1/97.0/89.6	85.2/86.5/97.0/86.8	90.1/92.4/99.3/95.2	92.1/92.7/97.7/90.7	88.2/98.2/98.2/91.5	97.6/98.0/99.1/93.7	88.4/91.2/97.8/89.9	96.5±1.8/96.8±1.5/99.5±0.0/95.2±0.5
macaroni2	61.7/60.2/93.9/78.3	70.9/69.6/97.3/90.5	82.5/86.3/98.4/85.8	87.2/88.0/96.6/84.9	81.2/82.2/97.0/87.2	87.2/89.2/97.4/87.6	78.1/80.6/96.9/87.1	82.1±2.7/78.2±4.3/99.2±0.2/95.6±0.8
capsules	63.4/78.4/94.8/69.0	86.8/91.5/97.1/77.0	93.7/96.5/98.1/89.0	89.0/94.3/98.2/85.1	80.6/89.8/96.8/72.4	90.1/95.0/98.5/85.8	90.5/96.0/97.9/85.2	97.0±0.8/98.3±0.5/98.2±0.3/95.5±0.7
candle	87.8/88.9/97.9/94.1	95.1/95.3/97.8/94.4	91.4/92.0/98.7/96.3	85.6/86.4/98.6/93.1	93.0/92.9/96.0/90.6	95.0/95.7/98.8/93.4	95.9/95.5/98.6/95.4	96.6±1.0/97.1±0.8/99.2±0.0/94.7±0.7
cashew	93.0/96.5/98.3/92.1	95.2/97.7/98.7/91.3	94.3/97.6/90.8/94.1	94.2/97.3/96.9/90.8	93.6/97.0/99.2/92.8	97.3/98.6/98.3/92.1	91.2/96.0/97.5/92.8	96.5±0.4/98.2±0.2/98.3±0.1/96.0±0.5
chewinggum	98.3/99.3/96.8/79.3	97.7/99.0/98.5/91.0	97.2/99.0/99.7/92.2	98.7/99.2/98.4/85.1	96.8/98.5/99.2/89.4	98.4/99.3/99.2/87.9	98.0/99.3/99.5/93.7	99.6±0.1/99.8±0.0/99.4±0.0/94.0±0.3
pipe_fryum	96.4/98.3/99.1/95.0	98.5/99.2/98.7/96.6	98.5/99.4/97.4/95.9	99.0/99.5/98.5/95.4	98.6/99.3/99.3/95.3	99.5/99.8/98.5/95.9	99.8/99.9/98.5/97.1	99.0±0.5/99.5±0.2/98.7±0.0/96.3±0.4
fryum	88.6/95.0/94.2/81.0	90.8/96.0/97.1/89.7	93.5/97.4/93.7/91.5	95.2/97.9/94.3/83.1	89.0/93.6/96.8/80.3	94.3/97.8/94.7/84.6	93.3/97.3/95.8/89.2	97.3±1.6/98.8±0.7/93.7±0.2/89.9±0.5
Mean	85.3/87.5/96.8/84.9	87.3/88.8/97.2/87.6	92.6/94.5/96.2/90.2	90.6/91.3/96.7/84.6	89.1/90.8/97.4/86.2	93.3/94.6/97.7/87.6	88.3/89.6/97.4/88.3	95.7±0.3/95.9±0.3/98.0±0.0/92.5±0.2

Table A10: Subset-wise performance comparison on VisA under 1-/2-/4-shot settings with AUROC, AP, pAUROC, and PRO metrics.

Category	1-shot				2-shot				4-shot			
	AUROC	AUPR	pAUROC	PRO	AUROC	AUPR	pAUROC	PRO	AUROC	AUPR	pAUROC	PRO
audiojack	56.3±3.1	41.3±5.2	94.7±0.5	77.5±1.4	59.8±2.3	40.8±1.2	95.7±0.8	81.0±3.1	68.6±5.3	51.0±9.7	97.2±0.7	86.7±2.9
bottle cap	75.8±0.8	62.6±1.0	98.4±0.2	92.2±0.8	79.4±4.5	68.8±8.6	98.7±0.5	93.4±2.4	83.0±4.4	76.0±9.1	99.1±0.6	95.4±3.0
button battery	77.8±2.4	83.7±1.6	96.2±0.4	85.8±0.9	79.2±1.8	84.5±1.0	96.6±0.2	86.6±1.6	81.2±2.9	86.0±2.3	97.2±0.5	87.8±3.0
end cap	65.9±1.1	73.4±1.1	96.9±0.2	90.9±0.5	72.0±3.5	77.3±3.6	97.3±0.2	92.1±0.6	76.9±2.7	80.7±3.3	97.8±0.4	93.4±1.0
eraser	86.8±1.8	83.5±2.3	99.5±0.1	97.7±0.1	87.9±0.6	84.3±1.7	99.6±0.0	97.9±0.3	89.7±1.3	86.2±1.2	99.7±0.0	98.2±0.2
fire hood	72.8±2.1	61.0±3.3	97.7±0.4	85.1±2.9	75.6±3.3	65.1±5.2	98.2±0.4	87.1±2.8	76.6±3.1	67.1±4.8	98.4±0.5	87.7±3.9
mint	69.5±2.5	68.8±2.3	94.4±0.5	72.3±5.8	69.3±0.8	68.7±1.5	94.7±1.2	71.8±3.9	71.0±1.6	69.9±3.0	94.6±1.5	70.0±5.4
mounts	64.2±3.4	55.6±4.0	96.6±0.7	87.6±5.2	67.3±6.5	58.8±6.4	96.9±1.0	88.5±5.3	80.4±1.0	71.1±1.4	98.4±0.4	92.4±3.1
pcb	61.9±0.9	70.5±1.4	95.8±0.1	84.1±0.4	68.6±4.0	77.5±4.9	96.7±0.6	86.7±2.0	76.5±5.6	84.0±5.4	97.6±0.6	89.7±2.2
phone battery	77.1±0.9	73.7±1.5	98.3±0.1	90.5±0.9	79.8±2.4	75.9±1.8	98.6±0.2	92.0±1.1	82.3±3.9	77.5±3.4	98.8±0.4	93.3±2.5
plastic nut	60.9±1.2	43.5±1.1	95.3±0.6	80.2±3.8	64.6±5.5	47.1±9.4	95.7±1.6	81.7±7.2	72.0±9.8	55.7±14.9	96.9±2.0	86.6±8.7
plastic plug	68.5±2.5	51.7±2.5	96.4±0.3	87.4±1.2	74.2±6.6	58.2±11.9	96.3±1.5	86.1±6.0	80.5±6.7	69.0±13.8	97.5±2.0	89.9±8.4
porcelain doll	73.1±2.0	62.7±3.0	96.7±0.5	86.7±2.4	74.1±2.3	63.0±3.5	97.2±0.8	88.2±3.2	77.6±4.9	66.4±5.3	97.8±1.0	90.6±4.6
regulator	48.4±2.3	25.0±0.9	91.7±0.4	67.2±2.0	54.5±7.3	30.0±7.5	93.0±2.5	71.2±9.7	58.6±7.2	36.1±11.1	94.4±3.3	76.3±13.0
rolled strip base	87.9±1.7	93.8±1.0	99.6±0.1	98.1±0.1	88.0±1.8	93.9±1.1	99.6±0.0	98.3±0.1	91.9±1.7	95.5±1.0	99.7±0.0	98.7±0.1
sim card set	83.7±4.2	87.5±3.6	99.2±0.1	94.7±1.0	86.9±4.7	89.9±3.8	99.2±0.1	95.0±0.7	90.0±5.0	92.2±3.8	99.3±0.1	95.3±1.0
switch	55.0±3.2	58.9±4.2	85.7±1.0	68.0±0.7	64.2±6.4	67.6±6.7	89.5±2.4	74.4±4.9	74.2±4.3	74.9±4.3	93.5±1.1	83.8±3.4
tape	92.5±1.6	89.6±2.4	99.4±0.1	97.8±0.5	93.3±1.1	90.4±1.2	99.4±0.1	97.8±0.3	94.2±1.0	91.5±1.5	99.5±0.1	98.1±0.4
terminalblock	57.3±3.7	56.6±6.2	96.9±0.6	88.8±1.6	64.0±4.6	61.1±4.4	97.7±0.5	91.7±1.4	66.9±8.2	62.0±6.4	97.7±0.8	91.8±2.4
toothbrush	59.7±1.2	65.5±0.9	82.9±2.1	67.1±0.8	64.9±3.7	69.3±3.0	87.2±3.1	72.2±3.7	74.1±7.8	77.7±7.8	91.7±2.3	79.8±4.8
toy	65.4±8.9	70.8±10.0	90.1±1.8	84.0±2.8	77.4±3.5	82.6±2.9	91.8±1.1	86.8±1.1	78.9±2.0	84.0±1.8	92.4±0.8	87.5±1.0
toy brick	68.6±2.1	61.6±3.7	94.8±0.3	72.5±3.5	71.3±2.2	65.3±3.4	95.5±0.4	75.1±3.3	72.3±1.6	66.4±2.5	95.7±0.3	75.4±2.5
transistor1	62.4±5.5	70.6±4.6	95.5±0.8	83.5±1.6	77.8±10.6	82.8±8.7	97.2±1.2	89.2±3.8	84.1±1.8	86.8±9.5	97.8±1.5	91.7±4.9
u block	70.9±1.9	54.6±2.0	97.7±0.7	87.4±3.4	71.4±3.4	56.5±5.7	97.4±0.8	86.0±3.6	74.8±4.0	60.0±5.8	97.8±0.9	87.8±4.9
usb	58.9±0.4	50.9±1.0	93.1±0.2	76.8±0.6	64.2±4.4	56.4±7.1	94.7±1.0	80.9±3.5	73.4±9.2	65.8±13.1	96.2±1.5	85.8±5.6
usb adaptor	56.8±1.5	44.4±2.5	94.1±0.6	75.3±1.9	59.2±3.1	45.9±3.0	94.7±1.4	77.1±5.2	67.2±3.9	59.0±6.0	97.0±1.1	84.2±5.0
vcpill	88.2±2.3	87.3±2.3	98.4±0.3	92.4±1.5	90.0±1.4	89.1±1.7	98.5±0.1	92.6±0.5	93.6±2.6	92.8±2.9	98.9±0.3	94.3±1.7
wooden beads	84.7±0.7	83.6±0.9	98.5±0.2	89.7±1.6	86.2±0.8	85.4±0.9	98.7±0.2	88.9±2.6	81.8±2.6	71.6±3.5	98.5±0.3	90.2±2.4
woodstick	81.8±0.9	71.7±1.8	98.3±0.2	90.8±0.7	81.0±2.1	70.3±2.3	98.4±0.4	89.9±2.4	81.8±2.6	71.6±3.5	98.5±0.3	90.2±2.4
zipper	92.3±1.7	95.9±1.0	97.6±0.4	93.5±0.8	94.1±2.3	96.9±1.3	98.0±0.6	94.6±1.8	95.9±2.1	97.8±1.1	98.4±0.4	95.7±1.5
Mean	70.8±1.2	66.7±1.5	95.7±0.3	84.9±0.7	74.7±1.2	70.1±1.7	96.4±0.3	86.5±1.1	79.1±2.1	74.7±2.3	97.3±0.3	88.9±1.4

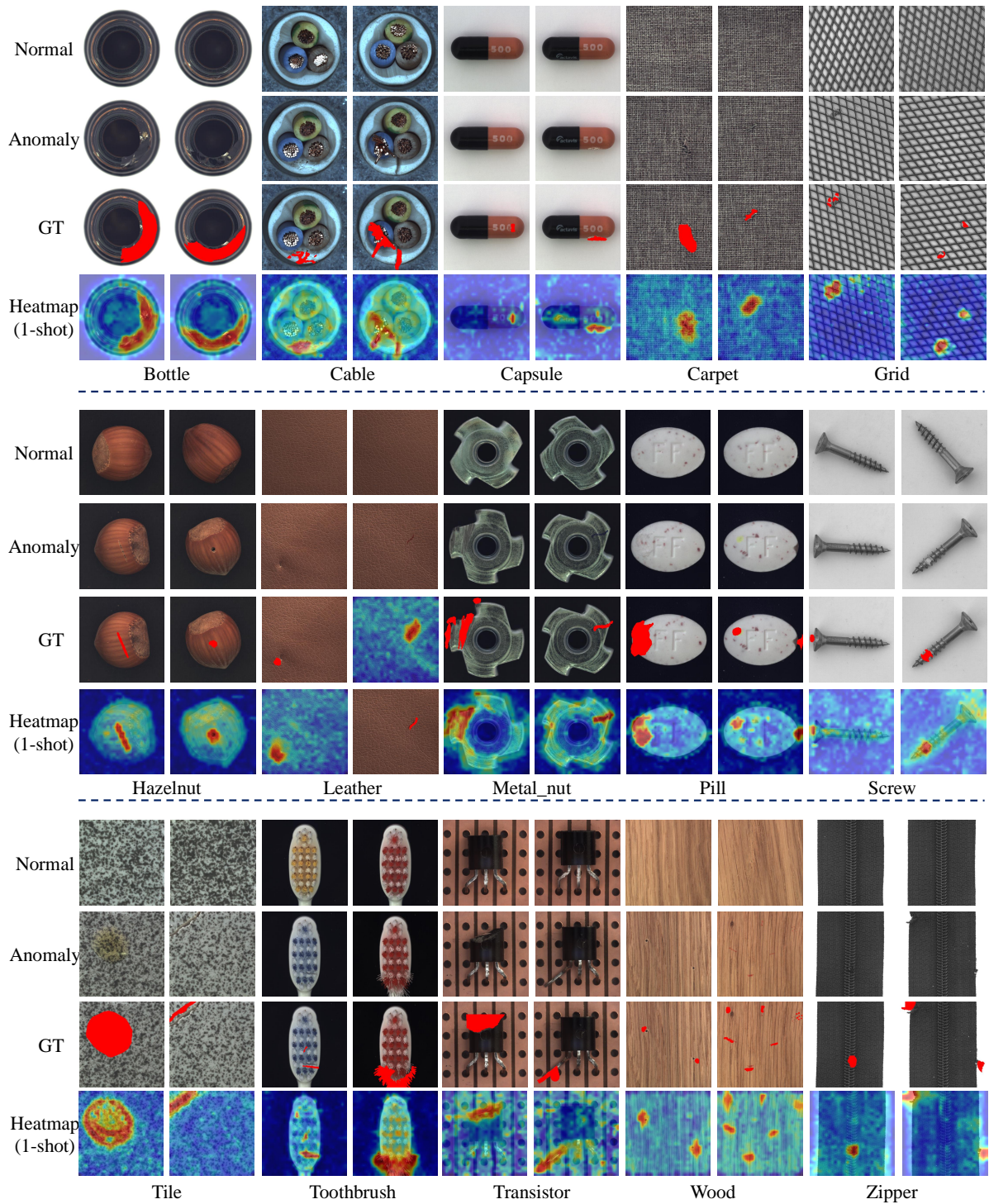


Figure A2: Additional qualitative 1-shot results of our method on MVTec. All samples are randomly selected.

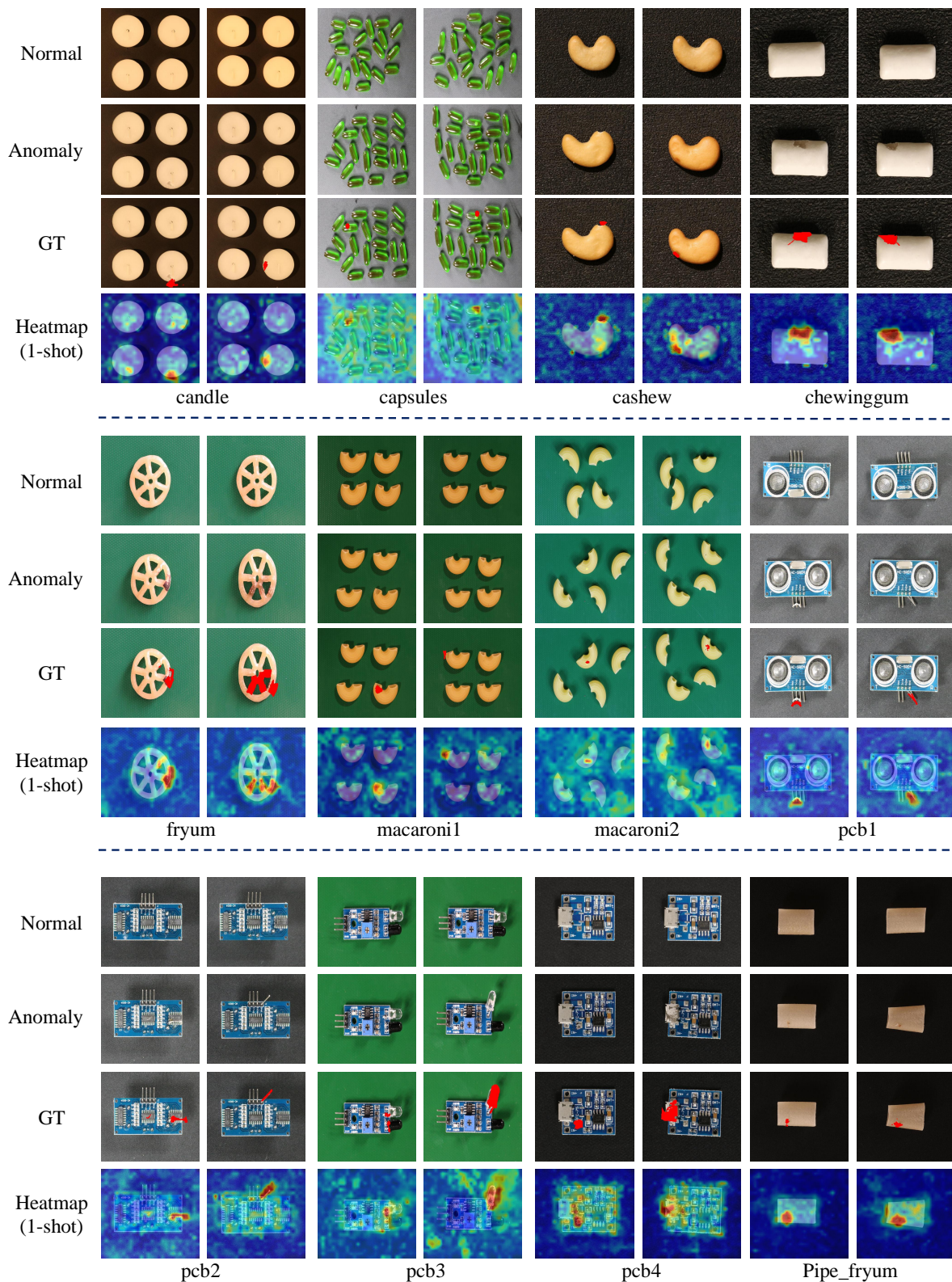


Figure A3: Additional qualitative 1-shot results of our method on VisA. All samples are randomly selected.

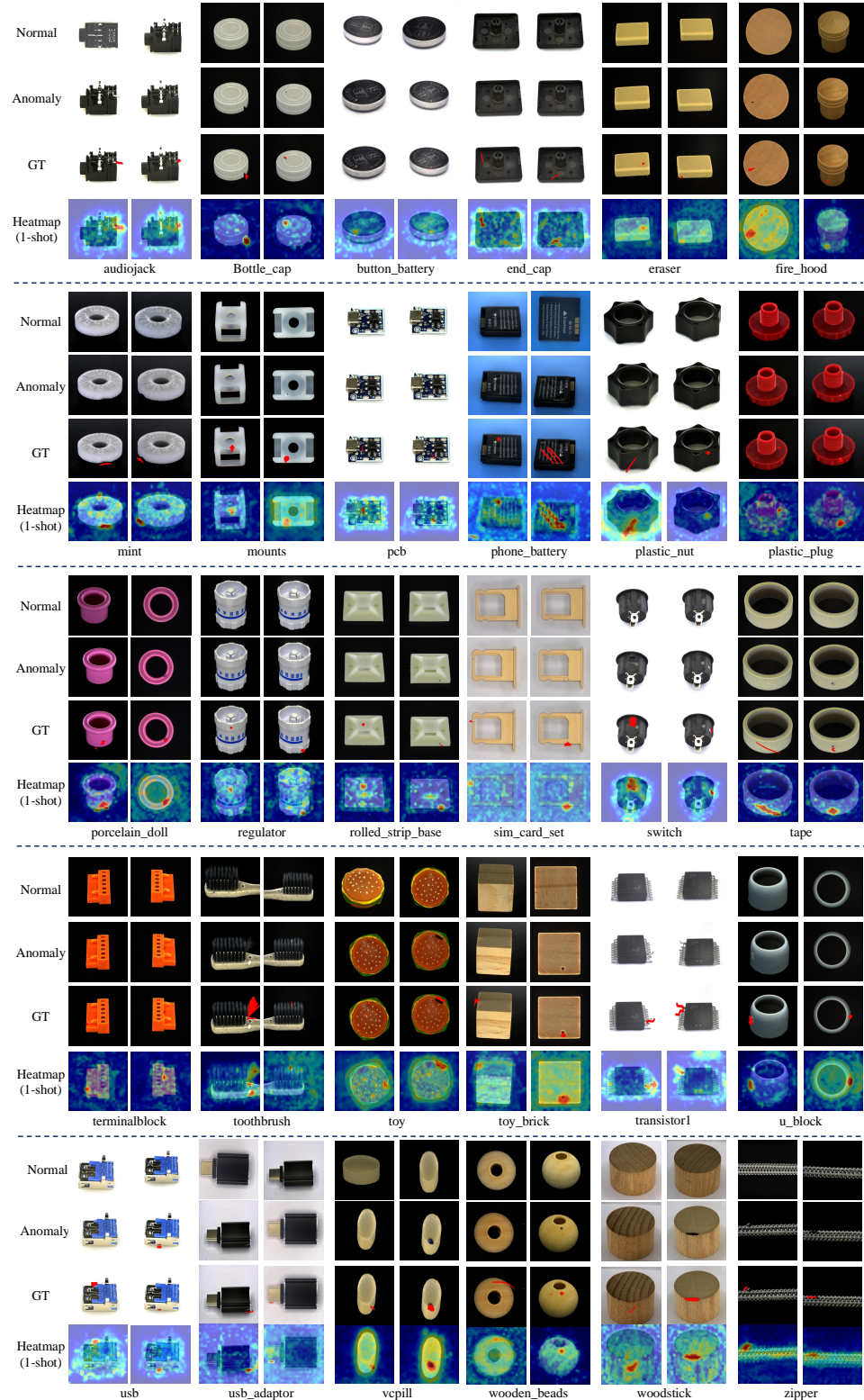


Figure A4: Additional qualitative 1-shot results of our method on Real-IAD. All samples are randomly selected.